Elsevier Editorial System(tm) for Journal of Volcanology and Geothermal Research

Manuscript Draft

Manuscript Number: VOLGEO2657R2

Title: Quaternary syn-collision magmatism from the Iran/Turkey borderlands

Article Type: Research Paper

Keywords: basalt; collision; volcanic; subduction; Iran

Corresponding Author: Dr Mark Allen,

Corresponding Author's Institution: University of Durham

First Author: Monireh Kheirkhah

Order of Authors: Monireh Kheirkhah; Mark Allen; Mohammad Emami

Abstract: Quaternary basaltic and andesitic lavas from the NW Iran/eastern Turkey border area are related to the active Arabia-Eurasia collision. The lavas occur within the Turkish-Iranian plateau, which ceased crustal thickening before the establishment of a number of volcanic centres within Iran and eastern Turkey, beginning at ~10 Ma. Models for generating syn-collision magmatism in eastern Anatolia have invoked slab-break-off beneath the thick crust and thin mantle lithosphere of the Cenozoic East Anatolia Accretionary Complex and/or partial loss of the lower lithosphere. Here we report geochemical and Sm-Nd/Rb-Sr data from a ~200 km long, N-S traverse that samples volcanic flows in NW Iran, many of which originate from centres in Turkey such as Ararat and Tendürek. Samples are transitional alkali/tholeiitic basalts and andesites. Ararat samples have lower Nb, lower large ion lithophile element (LILE) concentrations with 143Nd/144Nd ~0.51290. Other, volumetrically smaller, centres have higher Nb, higher LILE, with 143Nd/144Nd ~0.51265. Abundances of LILE and Nb increase from north to south. The presumed degree of partial melting increases in the opposite direction, away from the Arabia-Eurasia suture. Melting is inferred to have taken place in the spinel lherzolite field, largely from a continental lithosphere source influenced by

Mesozoic and early Cenozoic Neo-Tethyan subduction, but a separate source with long-term enrichment is needed to explain the high Nb, lower 143Nd/144Nd compositions.

Suggested Reviewers:

Quaternary syn-collision magmatism from the Iran/Turkey borderlands

M. Kheirkhah[a], M.B.Allen[b*], M. Emami[a]

[a]Research Institute for Earth Sciences, Geological Survey of Iran, Azadi Square, Meraj Avenue, Tehran, Iran

[b]Department of Earth Sciences, Durham University, Durham, DH1 3LE, UK

* Corresponding author;

m.b.allen@durham.ac.uk; tel: +44 (0)191 3342344; fax: +44 (0)191 3342301

Abstract

Quaternary basaltic and andesitic lavas from the NW Iran/eastern Turkey border area are related to the active Arabia-Eurasia collision. The lavas occur within the Turkish-Iranian plateau, which ceased crustal thickening before the establishment of a number of volcanic centres within Iran and eastern Turkey, beginning at ~10 Ma. Models for generating syn-collision magmatism in eastern Anatolia have invoked slab-break-off beneath the thick crust and thin mantle lithosphere of the Cenozoic East Anatolia Accretionary Complex and/or partial loss of the lower lithosphere. Here we report geochemical and Sm-Nd/Rb-Sr data from a ~200 km long, N-S traverse that samples volcanic flows in NW Iran, many of which originate from centres in Turkey such as Ararat and Tendürek. Samples are transitional alkali/tholeiitic basalts and andesites. Ararat samples have lower Nb, lower large ion lithophile element (LILE) concentrations with $^{143}Nd/^{144}Nd$ ~0.51290. Other, volumetrically smaller, centres have higher Nb, higher LILE, with $^{143}Nd/^{144}Nd$ ~0.51265. Abundances of LILE and Nb increase from north to south. The presumed degree of partial melting increases in

the opposite direction, away from the Arabia-Eurasia suture. Melting is inferred to have taken place in the spinel lherzolite field, largely from a continental lithosphere source influenced by Mesozoic and early Cenozoic Neo-Tethyan subduction, but a separate source with long-term enrichment is needed to explain the high Nb, lower $^{143}Nd/^{144}Nd$ compositions.

Keywords: basalt; collision; volcanic; subduction; Iran

1. Introduction

This paper describes Quaternary syn-collision magmatism in NW Iran, and compares it to volcanic rocks in adjacent centres in eastern Anatolia, Turkey. All of these volcanics (ranging from basalts through to rhyolites) lie within the Arabia-Eurasia collision zone, and are part of a much larger magmatic province which stretches from eastern Iran across to central and western Anatolia (partly shown on Fig. 1). Further west it merges with magmatism produced as a result of subduction at the Hellenic Trench. Our results extend knowledge of the collision zone magmatism eastward from the better-known centres in eastern and central Anatolia (Pearce et al., 1990, Notsu et al., 1995; Yilmaz et al., 1998; Keskin et al., 1998; Parlak et al., 2001; Sen et al., 2004; Özdemir et al., 2006), particularly for basalts from the major volcanoes Ararat and Tendürek. Such magmatism is a significant, regional, aspect of continental collision zones. By looking at an active example it is possible to use constraints that are not available for ancient, inactive settings, such as the lithosphere thickness at the time of melt generation and the precise relations between magmatism and the deformation pattern.

2. Geological setting

Northward motion of Arabia in the late Mesozoic and early Cenozoic was associated with subduction under the southern margin of Eurasia. The age of initial collision is disputed, with suggested ages ranging from ~10-12 Ma (Late Miocene, Dewey et al., 1986; McQuarrie et al., 2003) to ~35-40 Ma (Middle-Late Eocene; Hempton, 1987; Hessami et al., 2001; Vincent et al., 2005). Early deformation and changing sedimentation patterns on both sides of the Arabia-Eurasia (Bitlis-Zagros) suture indicate a Late Eocene age (~35 Ma), consistent with a sharp reduction in magmatism between the Eocene and Oligocene (Allen and Armstrong, 2008). Collision between the Arabian and Eurasian plates is active, shown by the complex seismicity of SW Asia, the GPS-derived velocity field and abundant evidence for neotectonic faulting in Iran, Turkey and adjacent countries (Jackson et al., 1995; Vernant et al., 2004). The Turkish-Iranian plateau (Fig. 1) is not undergoing major active crustal thickening (e.g. Berberian and Yeats, 1999), although earlier collision-generated thickening is indicated by both present Moho depths (commonly 45 – 60 km) and the record of mid Cenozoic compressional deformation (Allen et al., 2004). The plateau has typical elevations of 1.5-2 km, trailing off westwards in to western Turkey and eastwards in to the deserts of eastern Iran. Folding and thrusting are active at its margins, in ranges such as the Zagros and Alborz (Jackson et al., 1995), but far less so within the plateau interior. Active tectonics of NW Iran involve a counterclockwise rotating array of NW-SE trending, right-lateral strike-slip faults (Copley and Jackson, 2006).

Magmatism has occurred intermittently within SW Eurasia between the Oligocene and the present day, across much of the region north of the original suture (Fig. 1), and more rarely to the south, e.g. Karacalidag (Karacadag). Magmatism occurs predominantly within the Turkish-Iranian plateau, particularly since ~10 Ma (Keskin et al., 1998), although Damavand volcano lies within the Alborz mountains of northern Iran, north of the plateau (Davidson et al., 2004; Liotard et al., 2008). Local active tectonics involve right-lateral strike-slip faults and pull-apart basins, but there is no simple spatial relation between the basins and volcanic centres such as Ararat and Tendürek (Copley and Jackson, 2006). Keskin et al. (1998) identified three phases of Late Miocene-Pliocene magmatism across the Erzurum-Kars Plateau, which lies to the north of Mt Ararat. A series of central volcanoes is present in eastern Anatolia and NW Iran, including Ararat, Tendürek, Süphan, Nemrut and Yigit Dagi (Fig. 1). Many of these are dormant, although the youngest recorded eruption is from AD 1441 at Nemrut (Tchalenko, 1977). There are also cinder cones, either close to the major volcanoes, or apparently independent of them.

The nature and origins of this Late Cenozoic magmatism are still debated. The major element compositional variation is large, ranging from calc-alkali types resembling active continental margins to alkali basalts with typical within-plate characteristics (Pearce et al., 1990). Trace element characteristics also vary, from examples resembling supra-subduction zone rocks, to basalts resembling ocean island basalts. This variation has led to a variety of postulated source regions and melting regimes. Pearce et al. (1990) suggested lithosphere delamination as a trigger. Keskin (2003) invoked break-off of the slab of Neo-Tethyan oceanic crust beneath Eurasia, especially for the concentration of magmatism in eastern Anatolia. Both mechanisms

may occur (Keskin, 2007). The eastern Anatolian region is unusual, in that juvenile crust of the East Anatolian Accretionary complex may be underlain by asthenosphere without a significant amount of conventional lithospheric mantle (Zor et al., 2003; Şengör et al., 2003). However, Angus et al. (2006) used S-wave receiver function analysis to infer that the lithospheric thickness under eastern Anatolia is ~60-80 km (Fig. 1): thinner than average, but still implying several tens of kilometres thickness of mantle lithosphere beneath the crust of the region.

3. Samples and analytical techniques

Samples are from either the surfaces of exposed flows or the interior of flows exposed by incised river valleys. Many of the Quaternary lava flows within NW Iran originate across the political border in Turkey, arising in the central volcanoes of Little Ararat, Tendürek and Yigit Dagi (Fig. 1). Others derive from isolated cinder cones (some samples from Salmas, and the one sample from Gonbad), or are flows of uncertain origin that may arise from fissure-type eruptions within pull-apart basins (a sample from Siah Cheshmeh). The north-south distance from Ararat to Gonbad is about 200 km.

Ararat (Agri Dag) is a double-peaked composite volcano with summits of 5165 and 3903 m (Fig. 2). Samples were collected from lavas arising from the lower, eastern centre: Little Ararat. A few basaltic or andesite lava flows have travelled much further than the norm, up to 100 km in the case of one flow arising from Little Ararat, which flowed first southeast and then east. Such flows followed pre-existing valleys and gorges, producing narrow ribbons of lava confined to the valley floors.

Once an eruption ceased, drainage was re-established in the same river valleys (Fig. 2). Later incision has produced narrow gorges in these lava flows, typically on the scale of 5 – 20 m. Olivine + plagioclase ± clinopyroxene forms the essential mineral assemblage of both the basalt and andesite samples, with plagioclase (labradorite) predominant. Plagioclase laths are typically 0.5-1 mm long. Pyroxene is commonly acicular. Accessory minerals include magnetite and apatite. Small biotite grains are occasionally present. Textures are hyaloporphyritic, with olivine and plagioclase phenocrysts. Some of the rocks are vesicular. Alteration is minor, with some iddingsite and sericite. No evidence is seen for cumulate textures at outcrop or in thin-section; this is also true for the other centres in the study area. More petrographic data for Ararat and the other centres are presented in Kheirkhah (2007).

Tendürek is a composite volcano ~50 km south of Ararat, over 3500 m in altitude. Its summit lies within Turkey. The flows sampled in this study from the Chaldiran region correlate with a phase of basalt magmatism identified by Yilmaz et al. (1998) over an area of 500 km^2. Lavas followed pre-existing river valleys to reach >25 km east of the volcanic source. Samples possess fresh microlitic plagioclase, and microphenocrysts of olivine and clinopyroxene. Plagioclase grains have sieve texture. Titanomagnetite is an accessory phase. K-feldspar is present in the matrix. The rocks are finer-grained than at Ararat.

Basalts and hawaiites within the Siah Cheshmeh pull-apart basin are of uncertain origin: there is no evidence for flows travelling west-to-east along river valleys from any of the centres within Turkey. However, nor are they associated with any identified cinder cones. Textures are microlitic, porphyritic and trachytic.

Minerals are mainly plagioclase, olivine and microphenocryst of pyroxene in the matrix. Titanomagnetite forms an accessory phase. Xenocrysts of quartz are surrounded by reaction rims, typically including clinopyroxene. Alkali feldspar is present in the matrix. The rocks are not as fresh as the samples from Tendürek or Ararat.

Yigit Dagi is another composite volcano, located on the Turkey-Iran border, 130 km SSE of Tendürek, with an area of ~130 km^2. We are not aware of previous analyses from this centre. Its volcanostratigraphy has not been studied to the extent of other centres. The volcano is more dissected than others in the region, suggesting that has been inactive for longer. Basalt lava flows in the Salmas region lie over 25 km east of the summit of Yigit Dagi, and are dissected by modern drainage by up to ~100 m. Several basaltic cinder cones are also present in the Salmas region, and are aligned northwest- southeast. Textures in these rocks are highly variable, and include hyalo microlitic porphyry, intersertal and trachytic. Vesicles are common. The mineralogy is mainly plagioclase (with common sieve texture), clinopyroxene ± olivine. Phenocrysts of plagioclase (labradorite) and pyroxene occur in some flows. Amphibole phenocrysts and aggregates are present in some flows, but they are not common. Quartz xenocrysts are surrounded by pyroxene reaction rims. The matrix is glassy, with occasional microlitic K-feldspar. There is petrographic evidence for co-mingling of basic and acidic magma.

Three cinder cones in the Gonbad region are the southernmost volcanic centres in this study, 20 km south of Salmas, and also aligned northwest-southeast. Aa and pahoehoe flows are basaltic and basaltic andesite. Volcanic bombs are common.

Textures are hyalo-microlitic and porphyritic. Main minerals are clinopyroxene (augite and titanoaugite), plagioclase and olivine (commonly altered to magnetite, spinel and iddingsite). Amphibole is present in basaltic andesites. Matrices include biotite and K-feldspar and apatite.

3.1. Analytical techniques

Major and selected trace elements for 20 samples were analysed by a Philips PW1400 X-Ray fluoresence spectrometer with a Rhodium (Rh) tube, at the Department of Geology at the University of Leicester. Major elements were analysed on fused beads; trace elements on pressed powder briquettes. Full analytical procedures are in Tarney and Marsh (1991). A subset of ten samples was analysed for additional trace elements by Inductively Coupled Plasma Mass Spectroscopy (ICP-MS), using a Perkin Elmer-Sciex Elan 6000 in the Department of Earth Sciences at the University of Durham, following a standard nitric and hydrofluoric acid digestion (Ottley et al., 2003). Details of analyses for major and trace element standards are available on request.

Ten samples were analysed for Rb/Sr and Sm/Nd isotopes at the Department of Earth Sciences, University of Durham, using a ThermoElectron Neptune Multi-collector Plasma Mass Spectrometer (MC-ICP-MS). Sample preparation and analytical procedures follow Dowall et al. (2003) and Nowell et al. (2003). The average $^{143}Nd/^{144}Nd$ value obtained on pure and Sm-doped J&M internal Nd standard was 0.511111±0.000008 (16ppm 2SD; n=16). Sample data are reported relative to a J&M value of 0.511110 (equivalent to a La Jolla value of 0.511862). The average

201 $^{87}Sr/^{86}Sr$ value for international standard NBS987 was 0.710261±0.000007 (10ppm
202 2SD; n=9). Sample data are reported relative to an NBS987 value of 0.71024.
203
204 **4. Results**
205
206 Major and trace element data and Rb/Sr-Sm/Nd isotope values are presented in
207 Table 1. The majority of the samples have LOI <1%, consistent with the overall
208 freshness of the flows. On the total alkali versus silica diagram (Fig. 3a) most samples
209 plot within the alkali field and are basalts or hawaiites. There is a broad trend towards
210 increasing alkalinity to the south, i.e. the direction of the original Arabia-Eurasia
211 suture, with only samples from Little Ararat plotting in the sub-alkalic field. MgO
212 contents are too low for most of the basalts to be primary melts of mantle peridotite;
213 only one sample has MgO > 10% (Fig. 3b). Two minor flows from cinder cones and a
214 lava from the Salmas area have the most basic compositions, and are distinctly higher
215 in MgO than any of the analyses from the larger volcanoes at Ararat and Tendürek
216 (Fig. 3b). MgO, FeO_T and CaO all decrease with increasing SiO_2, consistent with the
217 fractionation of an assemblage of olivine ± pyroxene ± plagioclase (Fig. 3). Sr and Eu
218 show a poor negative correlation with SiO_2 (not shown), also suggesting plagioclase
219 fractionation. TiO_2 only declines in the most evolved (trachyandesite) rocks, i.e.
220 titanomagnetite fractionation appears to be unimportant through most of the
221 compositional range sampled. Y generally increases with SiO_2, except for the most
222 acidic, amphibole-bearing sample (Mu15.22), where it is lower than more basic
223 samples; this implies amphibole fractionation is not involved except for the most
224 evolved samples in the suite.
225

Representative primitive mantle-normalised variation diagrams ("spiderdiagrams") are presented in Fig. 4. Patterns in Fig. 4a and 4b are normalised to the primordial mantle composition of Sun and McDonough (1989). Patterns in Fig. 4c are normalised to the N-MORB values of Sun and McDonough (1989). The samples fall into two principal patterns, based on the relative abundance of large ion lithophile elements (LILE) and light rare earth elements (LREE) to heavy rare earth elements (HREE), and hence the steepness of the patterns from left to right across the spiderdiagram. This also shows in the REE data plotted in Fig. 4d. Flatter patterns are typical of lavas derived from Ararat. The steepest patterns are samples from the Siah Cheshmeh Basin (lava source unknown) or Salmas and Gonbad (both flows from Yigit Dagi and cinder cone eruptions). Within each group the spiderdiagrams are more or less parallel – reflecting a moderate amount of fractionation. None of the samples shows marked depletion in the heavy REE, which would have indicated the presence of garnet in the mantle source – i.e. the melting is likely to have taken place at relatively shallow depths, ≤80 km.

All samples show a negative Nb, Ta anomaly (Fig. 4c), implying the presence of a subduction-modified component in the mantle source and/or crustal contamination. Note that with the exception of the samples from Ararat, Nb values are relatively high, >25 ppm. The samples reported in this study display an unusually large range in La and Nb values, compared with published datasets from eastern Turkey (Fig. 5). La/Nb ratios vary between 1.3 and 2.5, and are consistently higher than 1. Figure 5 emphasises that the variation between centres is greater than within individual centres, with Tendürek having lower La/Nb values than Ararat, and Ararat

250 having lower values than either the lava flows or cinder cones represented in the Yigit
251 Dagi – Siah Cheshmeh – Salmas and Gonbad data.
252
253 Figure 6 shows Th/Yb versus SiO_2 for the subset of our samples with ICP-MS
254 data and equivalent samples from the literature on Ararat and Tendürek. There is a
255 positive correlation between Th/Yb and SiO_2 for Ararat and Tendürek, which suggests
256 the operation of combined assimilation-fractional crystallisation (AFC), as suggested
257 for Tendürek by Pearce et al. (1990).
258
259 On the plot of Nb/Y versus Zr/Y (Fig. 7), samples from the south (Gonbad and
260 Salmas) possess the highest ratios and those from Little Ararat the lowest. The array
261 neither overlaps nor lies parallel to the MORB or Icelandic Volcanic Zone fields
262 (Fitton et al., 1997). Nor does it trend towards the composition of typical continental
263 crust. Excess or deficiency of Nb relative to the lower boundary of the Icelandic array
264 can be expressed as
265
266 $$\Delta Nb = 1.74 + \log(Nb/Y) - 1.92\log(Zr/Y)$$
267
268 with positive values for excess and negative for deficiency.
269
270 ΔNb is a source characteristic of basaltic rocks, and insensitive to the degree
271 of partial melting, source depletion via melt extraction, crustal contamination,
272 fractionation or alteration (Fitton et al., 1997). The spread of data in Fig. 7 across the
273 Icelandic array boundary indicates a range of source compositions, from the southern,
274 Yigit Dagi-Siah Cheshmeh-Salmas-Gonbad group lying on or just above the lower

Iceland boundary (positive ΔNb) to the Ararat samples lying below it (negative ΔNb). Tendürek rocks have a linear trend sub-parallel to the lower bound of the Icelandic array, indicating a range in the degree of melting. A similar trend is visible in the Yigit Dagi-Siah Cheshmeh-Salmas-Gonbad, displaced to higher ΔNb. The Ararat data are more clustered.

The relationship between ΔNb and the latitude of the volcanic centres is highlighted on Fig. 8. This is roughly equivalent to plotting ΔNb versus distance from the Arabia-Eurasia suture, which runs WNW-ENE to the south of the study area (Fig. 1), but with the advantage that the latitude is a more precise measurement. Fig. 8 clearly shows that a positive ΔNb source characterises the magmatism in the south of the study area, closest to the suture, whereas centres to the north have negative ΔNb and a greater spread of ΔNb values. In the case of Ararat, this is from ~0 to -0.5. Data from the Nemrut and Mus centres (Fig. 1) are included in Fig. 8 as they lie close to our study area, and fill a gap in the latitude range.

The ten samples analysed for Sr and Nd isotopes are plotted on Fig. 9. The $^{143}Nd/^{144}Nd$ values range between ~0.512627 and ~0.512923 and $^{87}Sr/^{86}Sr$ ranges between 0.70461 and 0.705705, thus placing the sample array close to Bulk Silicate Earth (BSE) on the $^{143}Nd/^{144}Nd$ versus $^{87}Sr/^{86}Sr$ plot. The highest $^{143}Nd/^{144}Nd$ and lowest $^{87}Sr/^{86}Sr$ samples are from Little Ararat, at the northern geographical limit of the study area. The lowest $^{143}Nd/^{144}Nd$ values are from the Salmas region in the south of the study area, but two samples from Tendürek-derived flows have the highest $^{87}Sr/^{86}Sr$ values. There is little evidence in the isotopic values for crustal contamination: there is no marked trend towards high $^{87}Sr/^{86}Sr$ values (Fig. 9).

However, there are no analyses for any samples with SiO_2 >53%. Pearce et al. (1990) found higher Th/Yb ratios and positive correlations between $^{87}Sr/^{86}Sr$ and SiO_2 for more silicic volcanic rocks in eastern Turkey, indicating a component of crustal contamination in the evolved magmas. Keskin et al. (2006) used Pb isotope characteristics to identify crustal contamination by different crustal blocks in more evolved, mainly Late Miocene lavas from the Kars-Erzurum plateau, north of the Quaternary centres in this study. Again, this was more pronounced in evolved samples than the most basic lavas.

There is a striking relationship between $^{143}Nd/^{144}Nd$ and ΔNb, highlighted on Fig. 10, with the samples falling between positive ΔNb, low $^{143}Nd/^{144}Nd$ compositions in the south and negative ΔNb, high $^{143}Nd/^{144}Nd$ values in the north (Ararat).

5. Discussion

There is a difference in composition within the study area between lower-LILE compositions from Ararat and higher-LILE compositions from all the other centres sampled (Fig. 4). Tendürek lavas are more subtly different from the other centres, with relatively high Zr, TiO_2 and $^{87}Sr/^{86}Sr$, and low La/Nb. On the alkali versus silica plot (Fig. 3a), published analyses for evolved samples from Ararat and Tendürek diverge with increasing SiO_2, with the Tendürek rocks showing a much greater enrichment in alkali content at more acidic compositions (Pearce et al., 1990). Pearce et al. (1990) also noted the higher MgO and CaO for a given silica content in the Ararat as compared to the Tendürek lavas; this is also clear on Fig. 3.

The major element compositional changes between different centres is broadly consistent with what Keskin (2003) summarises for the eastern Turkish volcanics, where he describes an increase in alkalinity to the south. It is less clear that there is a decrease in a subduction component in the same direction, as suggested by Keskin (2003), given that La/Nb ratios do not systematically decline between Ararat and Gonbad, or across the other volcanic centres shown in Fig. 5. All but one of the centres north of the suture zone have La/Nb > 1, indicating an inherited subduction component and/or crustal contamination. As the signature is present in the most primitive samples in each centre, we think it unlikely that these ratios are only the result of contamination.

The exception to this pattern is the Sivas pull-apart basin along the Central Anatolian Fault Zone, in eastern Anatolia (Fig. 1; Parlak et al., 2001). This basin is ~200 km north of the Arabia-Eurasia suture at this longitude. Pliocene-Quaternary alkali basalt flows have La/Nb ratios of ~1 or <1, decreasing with inferred decrease in the amount of partial melting. Melting during the strike-slip faulting and associated local extension tapped a mantle source without the regional subduction signature. The Karacalidag volcanics to the south of the suture also possess a within-plate signature, with La/Nb ~1, indicating no subduction influence in the melt source.

None of the samples from this study possess the HREE depletion distinctive of melting in the garnet stability field (Fig. 4d). This is consistent with other volcanic centres located north of the Arabia-Eurasia suture, with the exception of Sivas (Parlak et al., 2001), where HREE values are low (Yb and Lu ~6 x chondritic values). These data were used by Parlak et al. (2001) to infer melting of asthenosphere in the garnet

stability field. Lavas from south of the suture at Karacalidag also have low HREE contents, and have been modelled as deriving from melts in the garnet stability field (>80 km) (Pearce et al., 1990).

There is considerable variation in ΔNb in our sample set, and a correlation between ΔNb and latitude (Figs. 7 and 8), roughly equivalent to distance from the Arabia-Eurasia suture (Fig. 1). There is also a correlation between ΔNb and $^{143}Nd/^{144}Nd$ (Fig. 10). These results suggest that two sources contributed to the Quaternary centres, dominantly a positive ΔNb, low $^{143}Nd/^{144}Nd$ source in the south and a negative ΔNb, high $^{143}Nd/^{144}Nd$ source in the north. We suggest there are variable contributions to the melts from a subduction-modified component (negative ΔNb) and a small melt fraction component (positive ΔNb). The former is presumably the subduction-modified mantle lithosphere reservoir already identified in previous studies of the Turkish volcanics (e.g. Pearce et al., 1990; Keskin, 2003). As noted above, there seems to be some of this component in all the eastern Anatolian and NW Iranian centres, given that La/Nb is consistently >1. The positive ΔNb component is something else. The low $^{143}Nd/^{144}Nd$ signature of these positive ΔNb rocks is inconsistent with simple small-degree melting of the bulk asthenosphere beneath the modern volcanoes; it suggests a long-term (potentially >1 Ga) process of enrichment of the source. Both the origin of this source and its physical location are debatable. A lithosphere reservoir is likely, perhaps enriched over time by small melt fractions from the asthenosphere. But ocean island basalts (OIB) have been recorded with similar low $^{143}Nd/^{144}Nd$ values (less than Bulk Earth), e.g. Vidal et al. (1984), and pyroxenite or eclogite within the asthenosphere have been suggested as sources for some OIB (e.g. Kogiso et al., 2003).

375

376 It is notable that the alkali volcanoes Tendürek, Nemrut and Mus all possess negative
377 ΔNb signatures, with significant overlap of their ΔNb values with Ararat. Ararat has
378 been thought of as a "calc-alkali", arc-like volcano, with a distinctly different source
379 to Tendürek, Nemrut and Mus (Pearce et al., 1990). Pearce et al. (1990) proposed that
380 the latter were all from lithosphere sources with little or no subduction influences;
381 Keskin (2003) proposed that the main source was upwelling asthenosphere, with little
382 or no subduction component. If the <80 km melt depths proposed above are correct,
383 and the lithosphere structure of Angus et al. (2006) is correct, then this positive ΔNb
384 source should reside in the mantle lithosphere.

385

386 This identification of mantle sources does not address why melting takes
387 place. The two main models proposed are partial lithospheric delamination (Pearce et
388 al., 1990) and slab breakoff (Keskin, 2003). Both mechanisms involve ascent of
389 asthospheric mantle to replace the sinking material. These are not mutually exclusive
390 explanations (Keskin, 2006) (Fig. 11). Partial loss of the mantle lithosphere consistent
391 with regional tomographic results from the whole collision zone (Maggi and Priestley,
392 2005), which show a low shear wave velocity anomaly in the uppermost mantle
393 beneath the plateau. Slab breakoff under eastern Turkey is supported by a recent
394 tomographic study (Lei and Zhao, 2007). The inferred lithosphere thickness for
395 eastern Turkey of ~60-80 km, contrasts with 100-125 km for the Arabian plate and the
396 Iranian sector of the Turkish-Iranian plateau (Angus et al., 2006). The latter
397 thicknesses are normal for continental lithosphere, but imply a low mantle
398 lithosphere/crustal thickness ratio, given the elevated crustal thicknesses determined
399 for parts of the Iranian plateau (Paul et al., 2006). Therefore slab breakoff may have

enhanced the melting process beneath eastern Turkey and NW Iran, but on current data appears unlikely to be the sole trigger for magmatism across the entire collision zone. Likewise, the unusual lithospheric structure of the East Anatolian Accretionary Complex may have enhanced the generation of magmatism across eastern Anatolia and adjacent areas, but cannot explain the presence of magmatism in other regions. There are two possible candidates for the origin of the oceanic slab: it may have originated either from a subduction zone under the Pontide volcanic centre (Keskin, 2003), or from the main Neo-Tethyan subduction zone, before the collision of the Arabian plate (Barazangi et al., 2006). Fig. 11 shows the latter scenario.

Both the delamination and the slab breakoff model involve the ascent of asthenosphere, which is apparently at odds with the subduction-influenced chemistry of the observed volcanics – argued here and elsewhere as derived from largely lithospheric sources (e.g. Pearce et al., 1990). A possible explanation is that upwelling asthenosphere created an initial melt, but that the final chemistry of the erupted rocks is dominated by incompatible trace element-enriched melt derived from the overlying lithosphere.

6. Conclusions

The petrological, geochemical, isotopic and tectonic data presented and reviewed in this paper allow us to constrain better the nature and origin of the Quateranry, syn-collision magmatism across the Turkish-Iranian plateau. Compositions range from tholeiitic to alkali, broadly increasing in alkalinity towards the Arabia-Eurasia suture, to the south of the study area. This north-south alkalinity

425 trend is consistent with a decrease in the extent, and presumed volume, of lavas in the
426 same direction. The chemistry of all the samples in this study indicates a subduction
427 component, characterised by high La/Nb ratios and elevated LILE. There is no
428 decrease in the La/Nb ratio from north-to-south, despite elevated amounts of LILE
429 and steeper spiderdiagram patterns in the south.
430
431 We propose that all volcanic centres in eastern Anatolia and NW Iran, with the
432 exception of Sivas and Karacalidag (Fig. 1), are largely derived from melting of
433 continental lithosphere in the spinel lherzolite field (<80 km; Fig. 11), in a region
434 which lay above the Late Mesozoic – Early Cenozoic Neo-Tethyan subduction zone,
435 and/or a separate subduction zone that dipped beneath the Pontide arc of NE Turkey
436 (Keskin, 2003). This subduction produced the distinctive supra-subduction zone
437 chemistry seen in the Pliocene-Quaternary basalts of this study and previous work,
438 several tens of millions of years after subduction ended. A separate source is needed
439 for the low $^{143}Nd/^{144}Nd$, positive ΔNb rocks in the south of the study area. This is
440 likely to be volumetrically smaller, with long-term enrichment. We note that it is
441 possible that the two sources occur within the same volume of lithospheric mantle.
442 The degree of contribution of each source to a particular melt will be the combined
443 result of several factors, including i) the actual composition of each type of fusible
444 material, ii) the amount of each source type in a given mantle volume, iii) the amount
445 of overstep of the solidi that control the melting of each source type.
446
447 At Karacalidag and Sivas low HREE values and low La/Nb ratios in basalts
448 indicate deeper melting of a source similar to that of OIB (Fig. 11). This OIB-like
449 source may also lie in the continental lithosphere in Karacalidag, given that this area

450 is south of the Arabia-Eurasia suture and so not affected by the Tethyan subduction. It
451 could be at least part in the asthenosphere. The Sivas basalts are more confidently
452 assigned to an asthenospheric source, similar to OIB. The cause of melting on the
453 regional scale is related to either partial loss of the lower lithosphere, slab breakoff of
454 Tethyan oceanic lithosphere, or a combination of the two.
455

456 **7. Acknowledgements**

457

458 We thank Nick Marsh, Chris Ottley and Geoff Nowell for help with sample analyses.
459 The Director and staff of the Geological Survey of Iran are thanked for their scientific
460 and logistical support. Jon Davidson, Graham Pearson and Colin Macpherson
461 provided useful discussion. Andy Saunders and John Dixon provided extremely useful
462 reviews. MBA was supported by Durham research grant R050475; MK thanks the
463 Royal Society for a travel grant to the UK.
464

465 **8. References**

466

467 Allen, M., Jackson, J. and Walker, R., 2004. Late Cenozoic reorganization of the
468 Arabia-Eurasia collision and the comparison of short-term and long-term
469 deformation rates. Tectonics, 23: art. no. TC2008, doi: 10.1029/2003TC001530.
470 Allen, M.B. and Armstrong, H.A., 2008. Arabia-Eurasia collision and the forcing of
471 mid Cenozoic global cooling. Palaeogeography Palaeoclimatology
472 Palaeoecology, 265: 52-58, doi: 10.1016/j.palaeo.2008.04.021.

473 Angus, D.A., Wilson, D.C., Sandvol, E. and Ni, J.F., 2006. Lithospheric structure of
474 the Arabian and Eurasian collision zone in eastern Turkey from S-wave receiver
475 functions. Geophysical Journal International, 166: 1335-1346.
476 Barazangi, M., Sandvol, E. and Seber, D., 2006. Structure and evolution of the
477 Anatolian plateau in eastern Turkey. In: Y. Dilek and S. Pavlides (Editors),
478 Postcollisional tectonics and magmatism in the Mediterranean region and Asia.
479 Geological Society of America, pp. 463-473.
480 Berberian, M. and Yeats, R., 1999. Patterns of historical earthquake rupture in the
481 Iranian plateau. Bulletin of the Seismological Society of America, 89: 120-139.
482 Copley, A. and Jackson, J., 2006. Active tectonics of the Turkish-Iranian Plateau.
483 Tectonics, 25: doi 10.1029/2005TC001096.
484 Davidson, J. et al., 2004. The geology of Damavand volcano, Alborz Mountains,
485 northern Iran. Geological Society Of America Bulletin, 116: 16-29.
486 Dewey, J.F., Hempton, M.R., Kidd, W.S.F., Saroglu, F. and Şengör, A.M.C., 1986.
487 Shortening of continental lithosphere: the neotectonics of Eastern Anatolia - a
488 young collision zone. In: M. Coward and A. Ries (Editors), Collision Tectonics.
489 Special Publication of the Geological Society 19, London, pp. 3-36.
490 Dowall, D.P., Nowell, G.M. and Pearson, D.G., 2003. Chemical pre-concentration
491 procedures for high-precision analysis of Hf-Nd-Sr isotopes in geological
492 materials by plasma ionisation multi-collector mass spectrometry (PIMMS)
493 techniques. In: Holland, J.G. and Tanner, S.D. (Editors), Plasma Source Mass
494 Spectrometry: Applications and Emerging Technologies. The Royal Society of
495 Chemistry, Cambridge, pp. 321-337.
496 Emami, M.H., Sadeghi, M.M.M. and Omrani, S.J., 1993. Magmatic map of Iran.
497 Geological Survey of Iran, Tehran.

498 Fitton, J.G., Saunders, A.D., Norry, M.J., Hardarson, B.S. and Taylor, R.N., 1997.
499 Thermal and chemical structure of the Iceland plume. Earth and Planetary
500 Science Letters, 153: 197-208.
501 Hessami, K., Koyi, H.A., Talbot, C.J., Tabasi, H. and Shabanian, E., 2001.
502 Progressive unconformities within an evolving foreland fold-thrust belt, Zagros
503 Mountains. Journal of the Geological Society, London, 158: 969-981.
504 Jackson, J., Haines, A.J. and Holt, W.E., 1995. The accommodation of Arabia-Eurasia
505 plate convergence in Iran. Journal of Geophysical Research, 100: 15205-15209.
506 Keskin, M., 2003. Magma generation by slab steepening and breakoff beneath a
507 subduction-accretion complex: An alternative model for collision-related
508 volcanism in Eastern Anatolia, Turkey. Geophysical Research Letters, 30(24):
509 1-4.
510 Keskin, M., 2007. Eastern Anatolia: a hot spot in a collision zone without a mantle
511 plume. In: G.R. Foulger and D.M. Jurdy (Editors), Plates, Plumes, and Planetary
512 Processes. Geological Society of America, pp. 1-25.
513 Keskin, M., Pearce, J.A., Kempton, P.D. and Greenwood, P., 2006. Magma-crust
514 interactions and magma plumbing in a postcollisional setting: geochemical
515 evidence from the Erzurum-Kars volcanic plateau, eastern Turkey. In: Y. Dilek
516 and S. Pavlides (Editors), Postcollisional tectonics and magmatism in the
517 Mediterranean region and Asia. Geological Society of America, Special Paper
518 409, pp. 475-505.
519 Keskin, M., Pearce, J.A. and Mitchell, J.G., 1998. Volcano-stratigraphy and
520 geochemistry of collision-related volcanism on the Erzurum-Kars Plateau,
521 northeastern Turkey. Journal of Volcanology and Geothermal Research, 85:
522 355-404.

523 Kheirkhah, M., 2007. The Petrology and Geochemiscal studies on Quaternary basaltic
524 rocks in NW of Iran (Azerbaijan). PhD Thesis, Azad University, Tehran, 360
525 pp.
526 Kogiso, T., Hirschmann, M.M. and Frost, D.J., 2003. High-pressure partial melting of
527 garnet pyroxenite: possible mafic lithologies in the source of ocean island
528 basalts. Earth and Planetary Science Letters, 216: 603-617.
529 Lei, J.S. and Zhao, D.P., 2007. Teleseismic evidence for a break-off subducting slab
530 under Eastern Turkey. Earth and Planetary Science Letters, 257: 14-28.
531 Liotard, J.M. et al., 2008. Origin of the absarokite-banakite association of the
532 Damavand volcano (Iran): trace elements and Sr, Nd, Pb isotope constraints.
533 International Journal of Earth Sciences, 97: 89-102.
534 Maggi, A. and Priestley, K., 2005. Surface waveform tomography of the Turkish-
535 Iranian plateau. Geophysical Journal International, 160: 1068-1080.
536 McQuarrie, N., Stock, J.M., Verdel, C. and Wernicke, B., 2003. Cenozoic evolution
537 of Neotethys and implications for the causes of plate motions. Geophysical
538 Research Letters, 30: art. no. 2036 doi 10.1029/2003GL017992.
539 Nakamura, N., 1974. Determination of REE, Ba, Fe, Mg, Na and K in carbonaceous
540 and ordinary chondrites. Geochimica and Cosmochimica Acta, 38: 757-775.
541 Notsu, K., Fujitani, T., Ui, T., Matsuda, J. and Ercan, T., 1995. Geochemical Features
542 Of Collision-Related Volcanic-Rocks In Central And Eastern Anatolia, Turkey.
543 Journal of Volcanology and Geothermal Research, 64: 171-191.
544 Nowell, G.M., Pearson, D.G., Ottley, C. J., Schweiters, J. and Dowall, D., 2003.
545 Long-term performance characteristics of a plasma ionisation multi-collector
546 mass spectrometer (PIMMS): the ThernoFinnigan Neptune. In: Holland, J.G.
547 and Tanner, S.D. (Editors) Plasma Source Mass Spectrometry: Applications and

548 Emerging Technologies. The Royal Society of Chemistry, Cambridge, pp. 307-
549 320.
550 Ottley, C.J., Pearson, D.G. and Irvine, G.J., 2003. A routine method for the
551 dissolution of geological samples for the analysis of REE and trace elements via
552 ICP-MS. In: J.G. Holland and S.D. Tanner (Editors), Plasma Source Mass
553 Spectrometry: Applications and Emerging Technologies. Royal Society of
554 Chemistry., Cambridge, pp. 221-230.
555 Özdemir, Y., Karaoglu, O., Tolluoglu, A.O. and Gulec, N., 2006. Volcano
556 stratigraphy and petrogenesis of the Nemrut stratovolcano (East Anatolian High
557 Plateau): The most recent post-collisional volcanism in Turkey. Chemical
558 Geology, 226: 189-211.
559 Parlak, O., Delaloye, M., Demirkol, C. and Unlugenc, U.C., 2001. Geochemistry of
560 Pliocene/Pleistocene basalts along the Central Anatolian Fault Zone (CAFZ),
561 Turkey. Geodinamica Acta, 14: 159-167.
562 Paul, A., Kaviani, A., Hatzfeld, D., Vergne, J. and Mokhtari, M., 2006. Seismological
563 evidence for crustal-scale thrusting in the Zagros mountain belt (Iran).
564 Geophysical Journal International, 166: 227-237.
565 Pearce, J.A. et al., 1990. Genesis of collision volcanism in eastern Anatolia, Turkey.
566 Journal of Volcanology and Geothermal Research, 44: 189-229.
567 Sen, P.A., Temel, A. and Gourgaud, A., 2004. Petrogenetic modelling of Quaternary
568 post-collisional volcanism: a case study of central and eastern Anatolia.
569 Geological Magazine, 141: 81-98.
570 Şengör, A.M.C., Ozeren, S., Genc, T. and Zor, E., 2003. East Anatolian high plateau
571 as a mantle-supported, north-south shortened domal structure. Geophysical
572 Research Letters, 30: art. no. 8045 doi:10.1029/2003GL017858.

573 Sun, S.S. and McDonough, W.F., 1989. Chemical and isotopic systematics of oceanic
574 basalts: implications for mantle composition and processes. In: A.D. Saunders
575 and M.J. Norry (Editors), Magmatism in the Ocean Basins. Geological Society
576 of London Special Publication, pp. 313-345.
577 Tarney, J. and Marsh, N.G., 1991. Major and trace element geochemistry of Holes
578 CY-1 and CY-4: Implications for petrogenetic models. In: I.L. Gibson, J.
579 Malpas, P.A. Robinson and C. Xenophontos (Editors), Initial Reports, Holes
580 CY-1and CY-1A. Geological Survey of Canada, pp. 133-175.
581 Tchalenko, J.S., 1977. Reconnaissance of seismicity and tectonics at northern border
582 of Arabian plate (Lake Van region). Revue de Geographie Physique et de
583 Geologie Dynamique, 19: 189-207.
584 Vernant, P. et al., 2004. Contemporary crustal deformation and plate kinematics in
585 Middle East constrained by GPS measurements in Iran and northern Iran.
586 Geophysical Journal International, 157: 381-398.
587 Vidal, P., Chauvel, C. and Brousse, R., 1984. Large mantle heterogeneity beneath
588 French Polynesia. Nature, 307: 536-538.
589 Vincent, S.J. et al., 2005. Insights from the Talysh of Azerbaijan into the Paleogene
590 evolution of the South Caspian region. Bulletin of the Geological Society of
591 America, 117: 1513-1533.
592 Yilmaz, Y., Guner, Y. and Saroglu, F., 1998. Geology of the quaternary volcanic
593 centres of the east Anatolia. Journal of Volcanology and Geothermal Research,
594 85: 173-210.
595 Zor, E. et al., 2003. The crustal structure of the East Anatolian plateau from receiver
596 functions. Geophysical Research Letters, 30: art. no. 8044,
597 doi:10.1029/2003GL018192.
598

Figure captions

Fig. 1. a) Quaternary volcanic centres (black) and major faults in eastern Turkey and NW Iran. Grey areas are lakes. Areas sampled in this study are in italics. Derived from Pearce et al., (1990); Emami et al. (1993); Yilmaz et al. (1998); Parlak et al. (2001); Copley and Jackson (2006). b) Location of a). The white line indicates the approximate boundary to the Turkish-Iranian plateau. The white triangle is the location of Damavand volcano in the Alborz mountains. c) East-west lithosphere profile of Angus et al. (2006). d) North-south lithosphere profile of Angus et al. (2006).

Fig. 2. a) MrSID mosaic of Landsat imagery (bands 2,4,7) for the Ararat region, eastern Turkey and NW Iran. b) incised basalt lava at the western side of the Zang-e Mar gorge. Ararat samples in this study are flows to the east and southeast of Little Ararat.

Fig. 3. a) Total alkali versus SiO_2 plot for basic and intermediate lavas in NW Iran, sampled in this study (solid symbols) and from Ararat and Tendürek in Turkey (open symbols; data from Pearce et al., 1990; Notsu et al., 1995; Yilmaz et al., 1998; Sen et al., 2004; b) MgO versus SiO_2; c) CaO versus SiO_2; d) TiO_2 versus SiO_2. All values as weight %.

Fig. 4. Normalised multi-element plots ("spiderdiagrams") and REE plots. a) and b) Primordial mantle normalised spiderdiagrams for representative NW Iran basaltic samples: a) samples from Ararat; b) samples from other centres. Normalising values

are from Sun and McDonough (1989). c) N-MORB normalised spiderdiagram envelope for all samples analysed in this study. Normalising values are from Sun and McDonough (1989). d) Representative REE plots for samples from this study (Mu 16.23 and Mu 18.25), Sivas (S-42; Parlak et al., 2001) and Karacalidag (MA-8; Sen et al., 2004). SiO_2 as weight %. Normalising values from Nakamura (1974).

Fig. 5. La v Nb plot for Quaternary lavas from NW Iran (this study) and eastern Turkey. Previous analyses are rocks with MgO > 4% and SiO_2 < 60% from Pearce et al. (1990); Keskin et al. (1998); Yilmaz et al. (1998); Sen et al. (2004); Özdemir et al. (2006). All of the Turkish data are from Quaternary or Late Pliocene centres, with the exception of Late Miocene-Pliocene data from the Erzurum-Kars Plateau (Keskin et al., 1998). These rocks overlap closely the Central Anatolian field, and so are not separated. Values are in ppm.

Fig. 6. Plot of Th/Yb v SiO2 to show, qualitatively, the influence of AFC processes on the sample suite.

Fig. 7. Nb/Y v Zr/Y plot for Quaternary lavas in this study. Compositional fields from Fitton et al. (1997). See text for discussion.

Fig. 8. Plot of ΔNb versus latitude for Quaternary basalts and andesites from NW Iran (this study) and eastern Turkey (data sources as before), showing the decrease of ΔNb from south to north.

Fig. 9. $^{143}Nd/^{144}Nd$ v $^{87}Sr/^{86}Sr$ plot for Quaternary lavas from NW Iran (this study) and eastern Turkey (data sources as before).

Fig. 10. Plot of ΔNb versus $^{143}Nd/^{144}Nd$, showing the co-variation in these parameters and the existence of positive ΔNb, low $^{143}Nd/^{144}Nd$ and negative ΔNb, high $^{143}Nd/^{144}Nd$ end members.

Fig. 11. Schematic reconstruction for Quaternary volcanism across the Arabia-Eurasia collision zone and its foreland, in the region of NW Iran and eastern Turkey. Volcanic centre names are included to give examples for each setting of magmatism, and do not fall on a linear section line. Inset cartoons show spiderdiagrams of basalts derived from asthenosphere and mantle lithosphere sources.

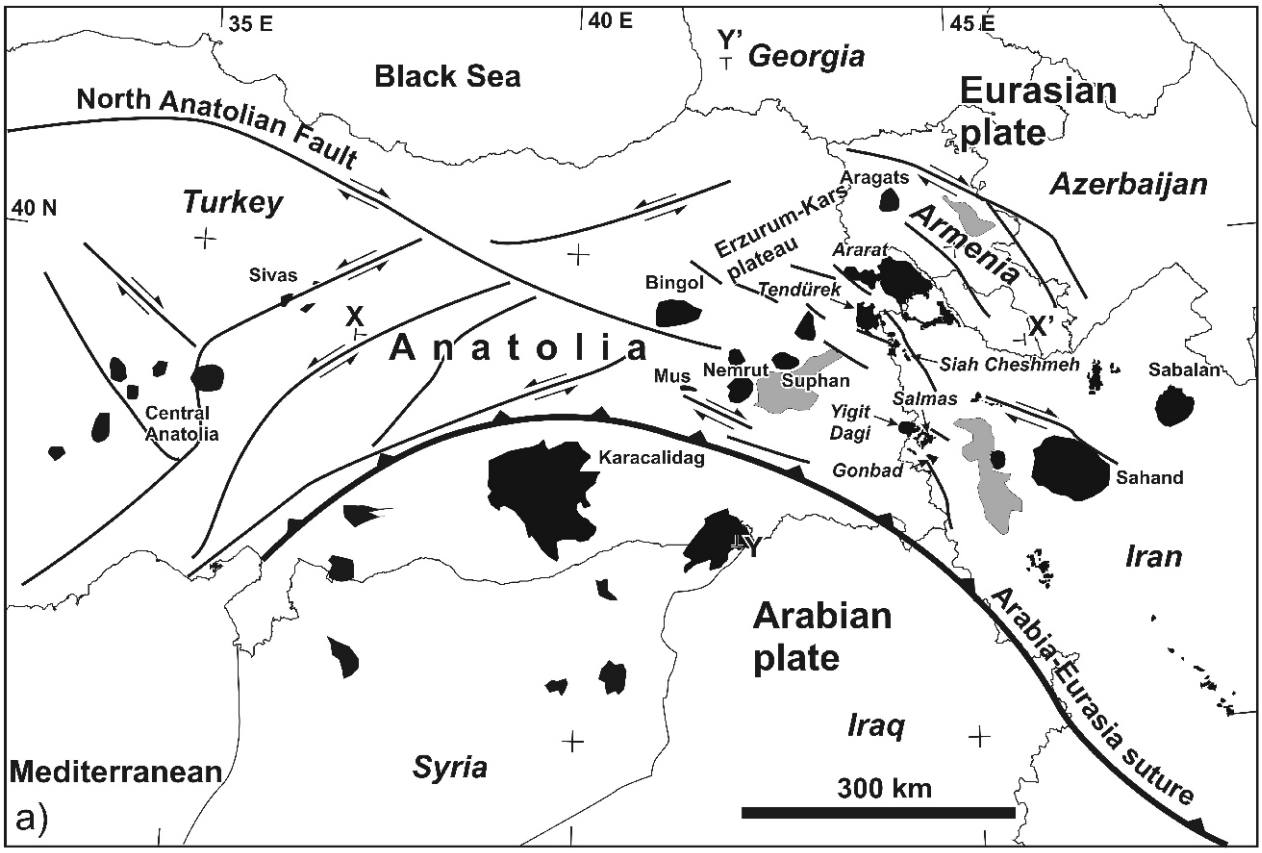
35 E
40 E
45 E
Y'
Georgia
Black Sea
North Anatolian Fault
Eurasian plate
Azerbaijan
40 N
Turkey
Aragats
Erzurum-Kars plateau
Armenia
Ararat
Bingol
Tendürek
Sivas
X
X'
Anatolia
Siah Cheshmeh
Sabalan
Mus
Nemrut
Suphan
Salmas
Yigit Dagi
Central Anatolia
Karacalidag
Gonbad
Sahand
Y
Iran
Arabian plate
Arabia-Eurasia suture
Iraq
Mediterranean
Syria
300 km
a)

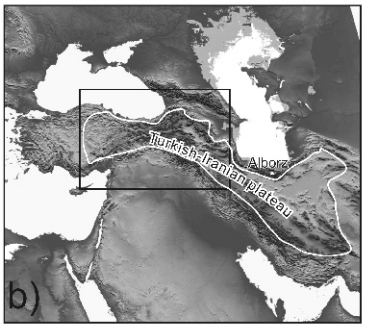
Turkish-Iranian plateau
Alborz
b)

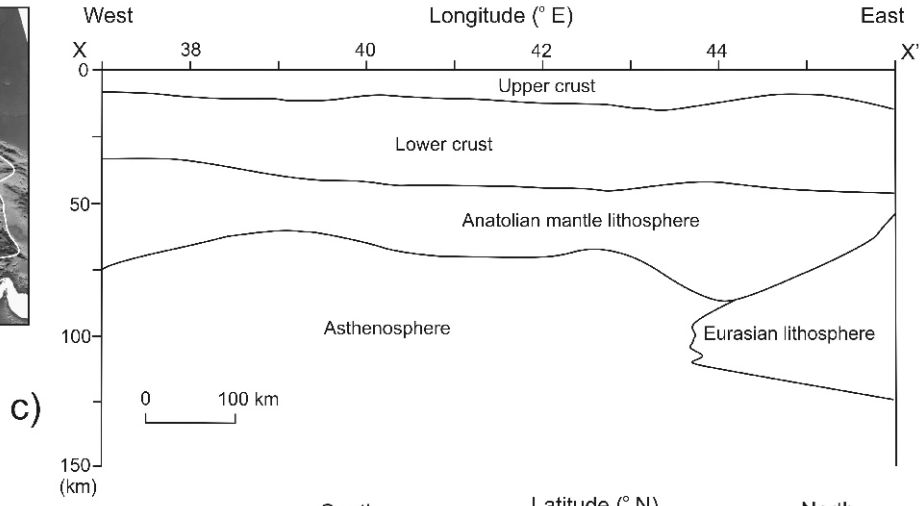
West
Longitude (° E)
East
X
38
40
42
44
X'
0
Upper crust
Lower crust
50
Anatolian mantle lithosphere
100
Asthenosphere
Eurasian lithosphere
0
100 km
c)
150
(km)

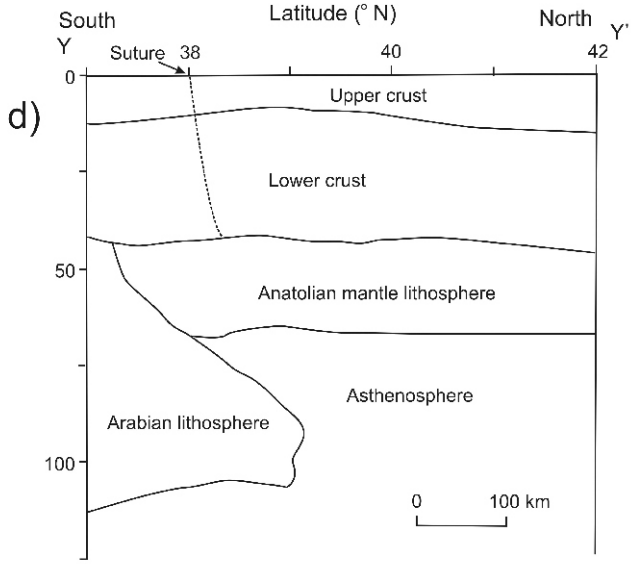
South
Latitude (° N)
North
Y
Y'
Suture
38
40
42
0
Upper crust
Lower crust
50
Anatolian mantle lithosphere
Asthenosphere
Arabian lithosphere
100
0
100 km
d)

Fig. 1

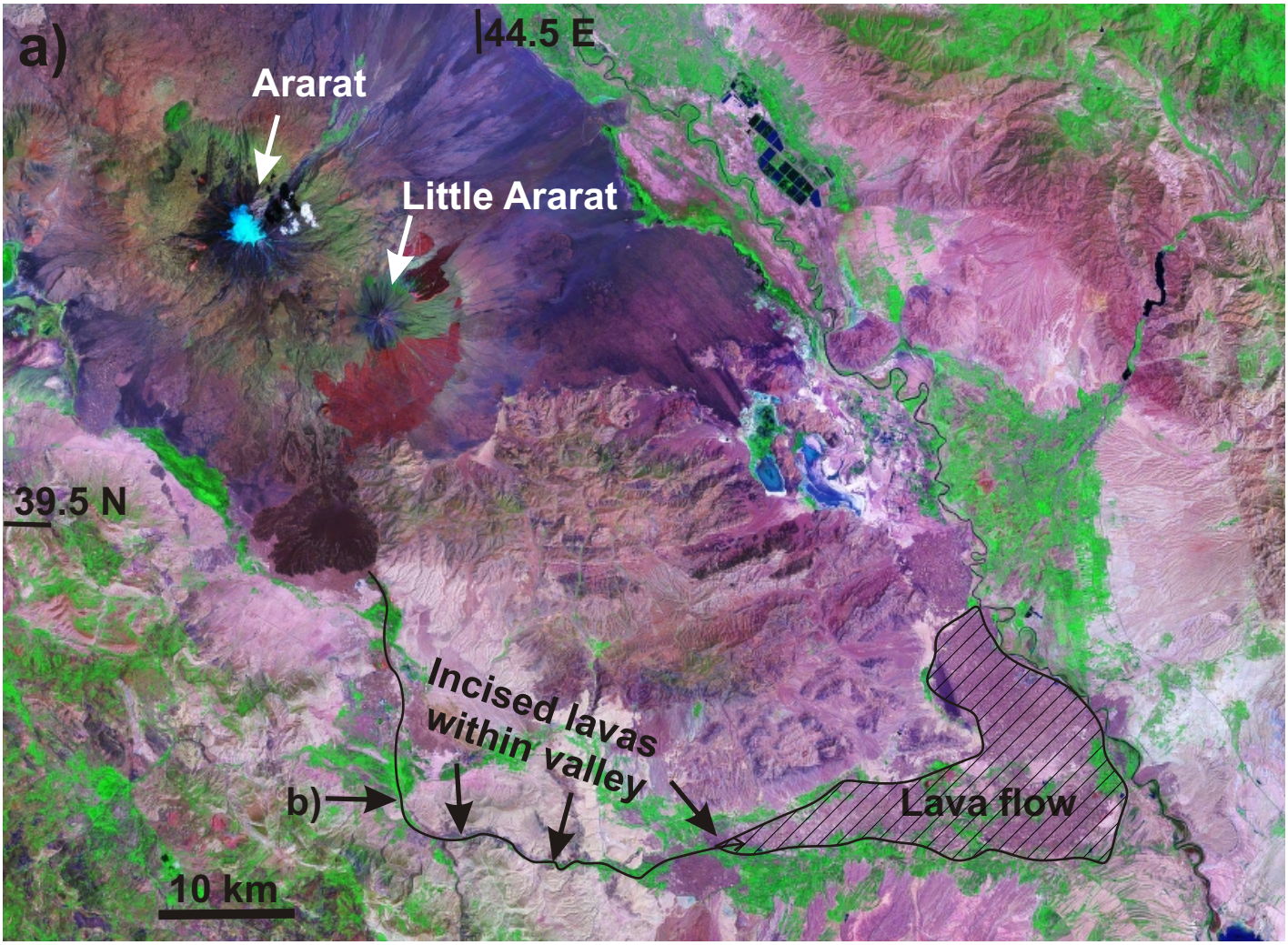
a)
44.5 E
Ararat
Little Ararat
39.5 N
Incised lavas within valley
b)
Lava flow
10 km


b)

Fig. 2

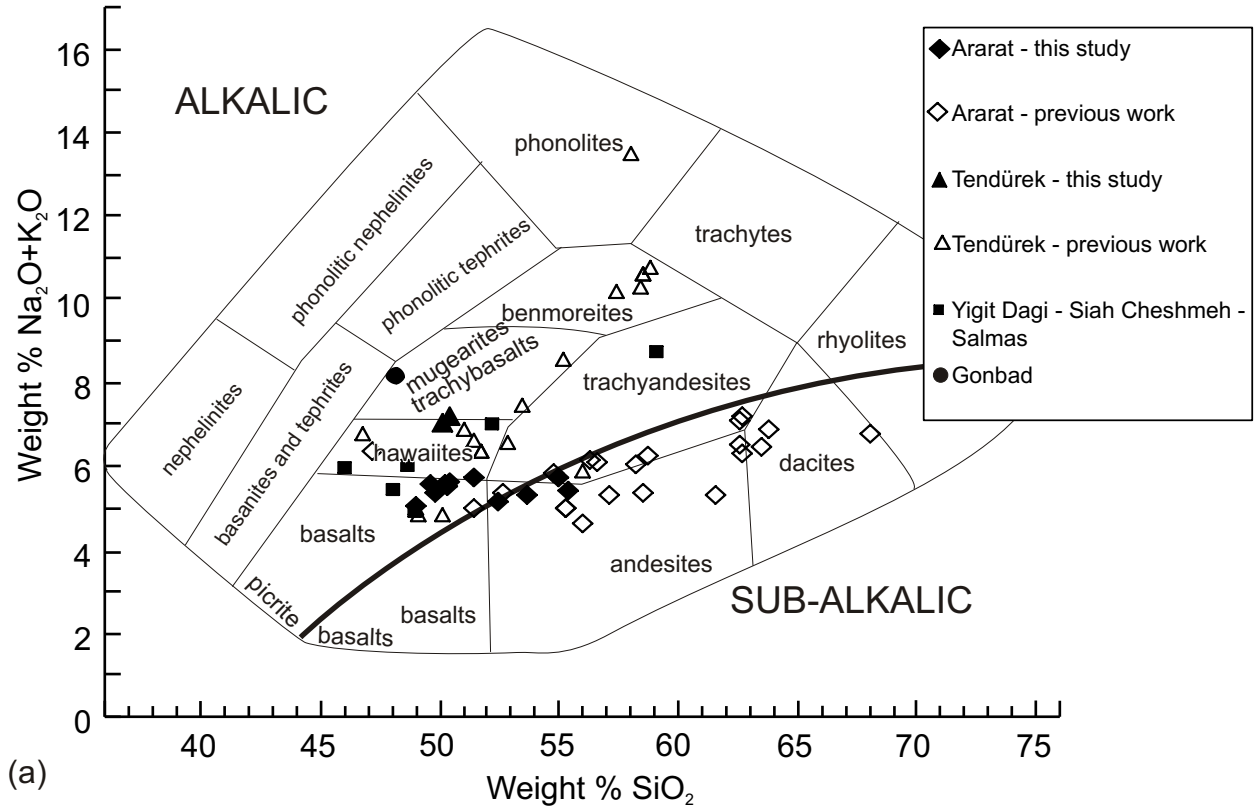
ALKALIC
SUB-ALKALIC
phonolites
trachytes
phonolitic nephelinites
phonolitic tephrites
benmoreites
rhyolites
mugearites
trachybasalts
trachyandesites
nephelinites
basanites and tephrites
hawaiites
dacites
basalts
andesites
picrite
basalts
basalts
Ararat - this study
Ararat - previous work
Tendürek - this study
Tendürek - previous work
Yigit Dagi - Siah Cheshmeh - Salmas
Gonbad
Weight % Na2O+K2O
Weight % SiO2
(a)

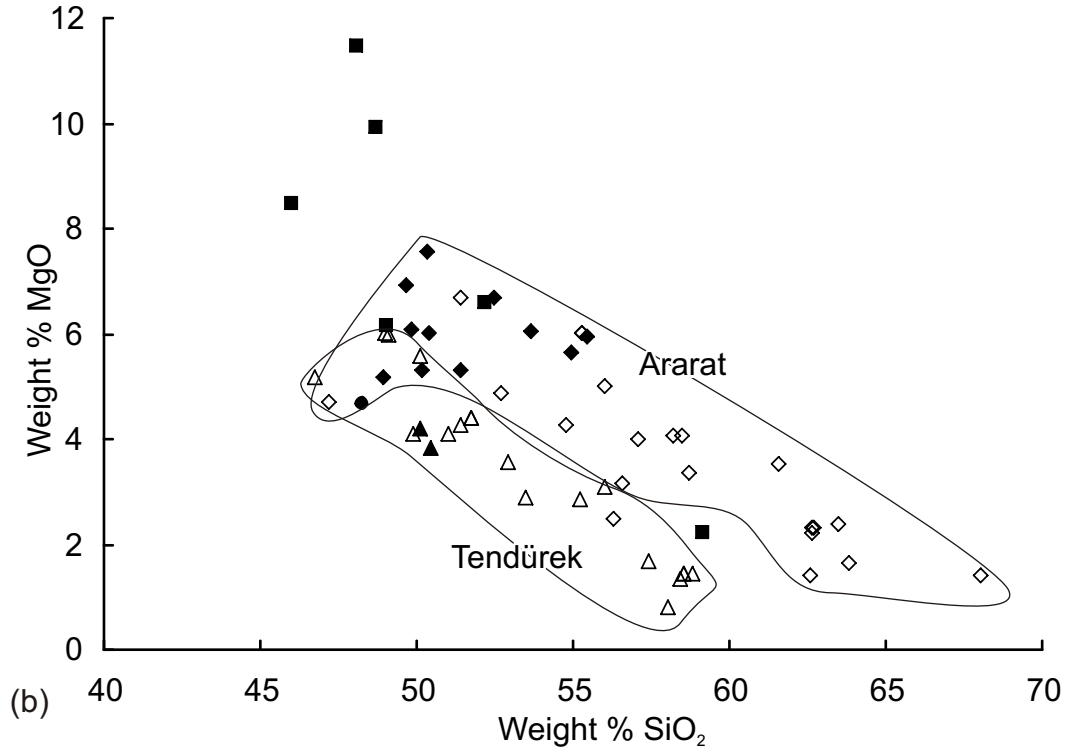
Ararat
Tendürek
Weight % MgO
Weight % SiO2
(b)

Fig. 3a & b

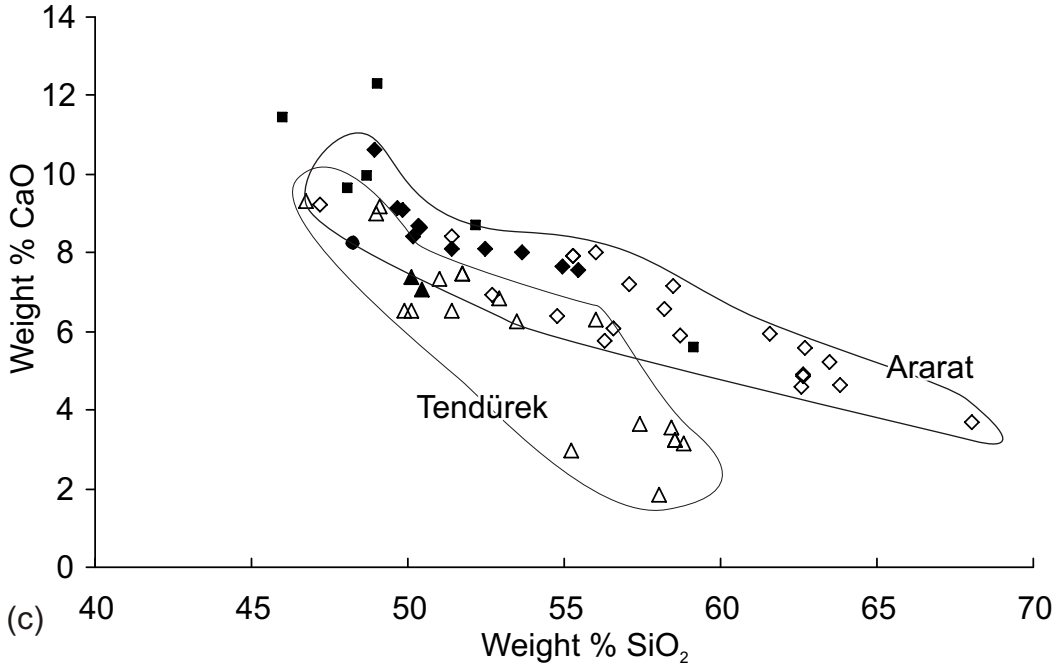
Weight % CaO
Weight % SiO2
Ararat
Tendürek
(c)

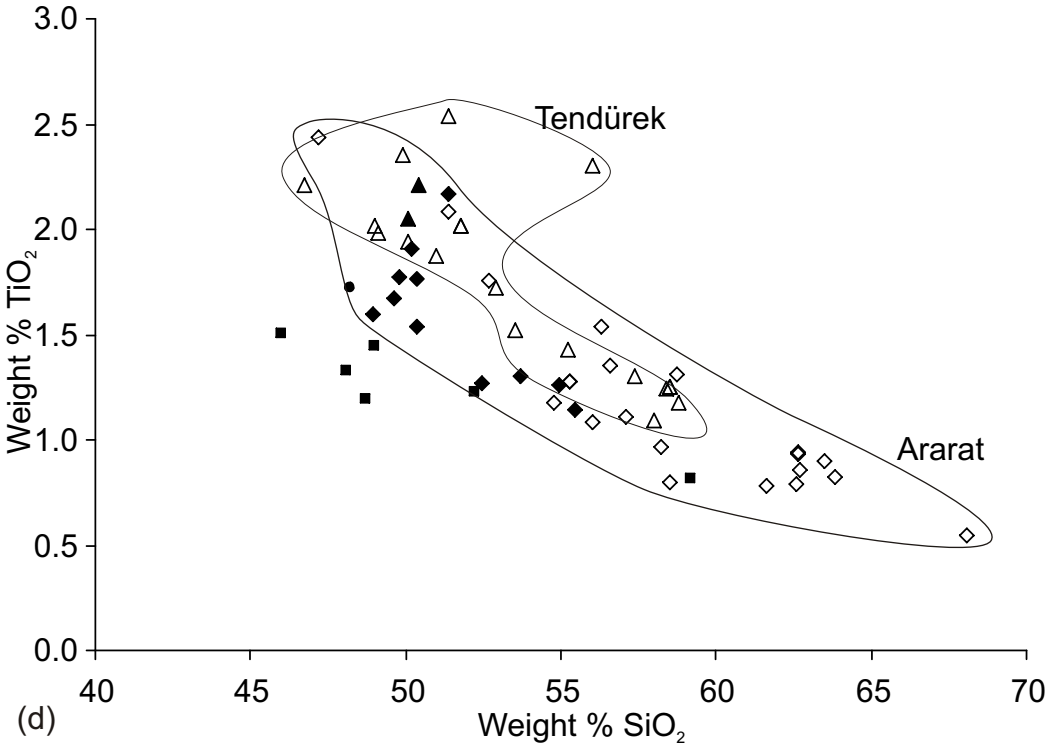
Weight % TiO2
Weight % SiO2
Tendürek
Ararat
(d)

Fig. 3c & d

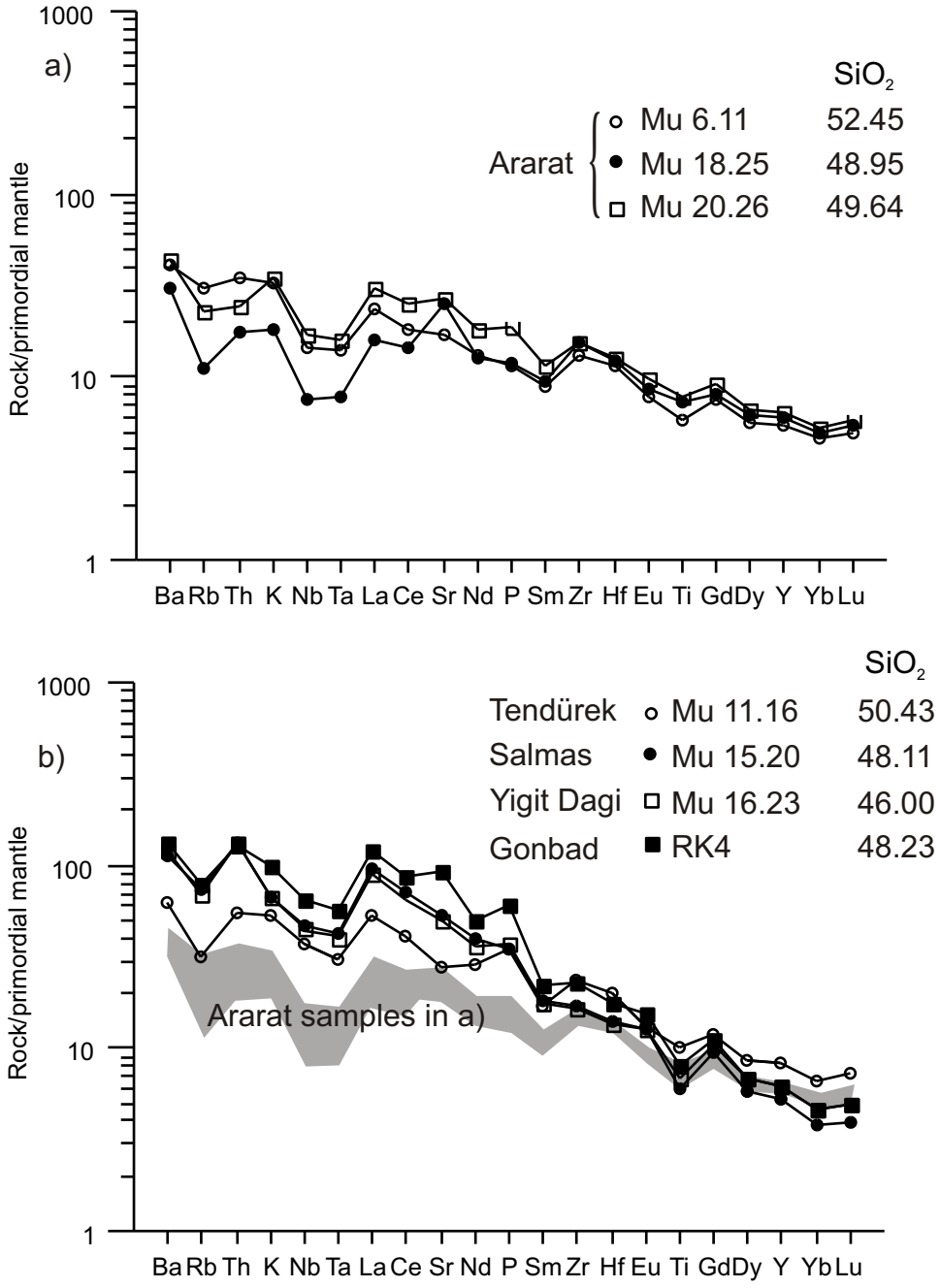
a)
1000
100
10
1
Rock/primordial mantle
SiO2
Ararat
Mu 6.11 52.45
Mu 18.25 48.95
Mu 20.26 49.64
Ba Rb Th K Nb Ta La Ce Sr Nd P Sm Zr Hf Eu Ti Gd Dy Y Yb Lu
b)
1000
100
10
1
Rock/primordial mantle
SiO2
Tendürek Mu 11.16 50.43
Salmas Mu 15.20 48.11
Yigit Dagi Mu 16.23 46.00
Gonbad RK4 48.23
Ararat samples in a)
Ba Rb Th K Nb Ta La Ce Sr Nd P Sm Zr Hf Eu Ti Gd Dy Y Yb Lu

Fig. 4a & b

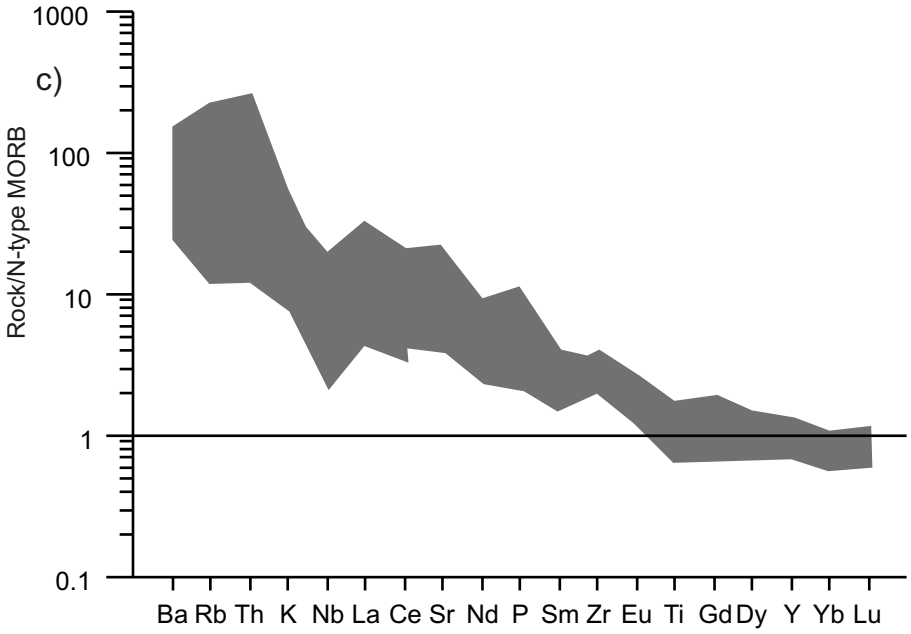
c)
Rock/N-type MORB
1000
100
10
1
0.1
Ba Rb Th K Nb La Ce Sr Nd P Sm Zr Eu Ti Gd Dy Y Yb Lu

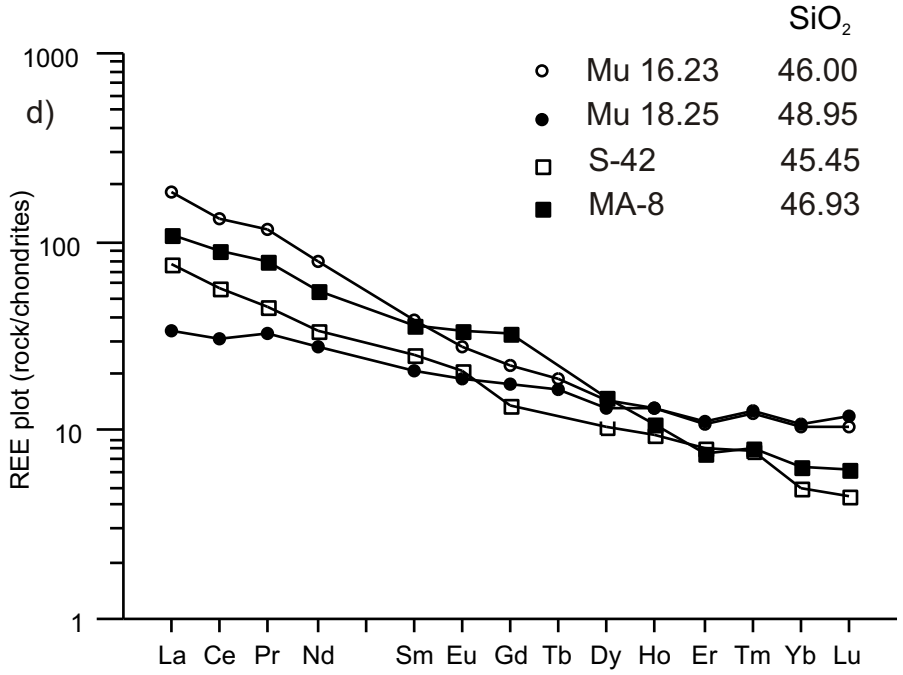
d)
REE plot (rock/chondrites)
1000
100
10
1
SiO2
Mu 16.23 46.00
Mu 18.25 48.95
S-42 45.45
MA-8 46.93
La Ce Pr Nd Sm Eu Gd Tb Dy Ho Er Tm Yb Lu

Fig. 4 c & d

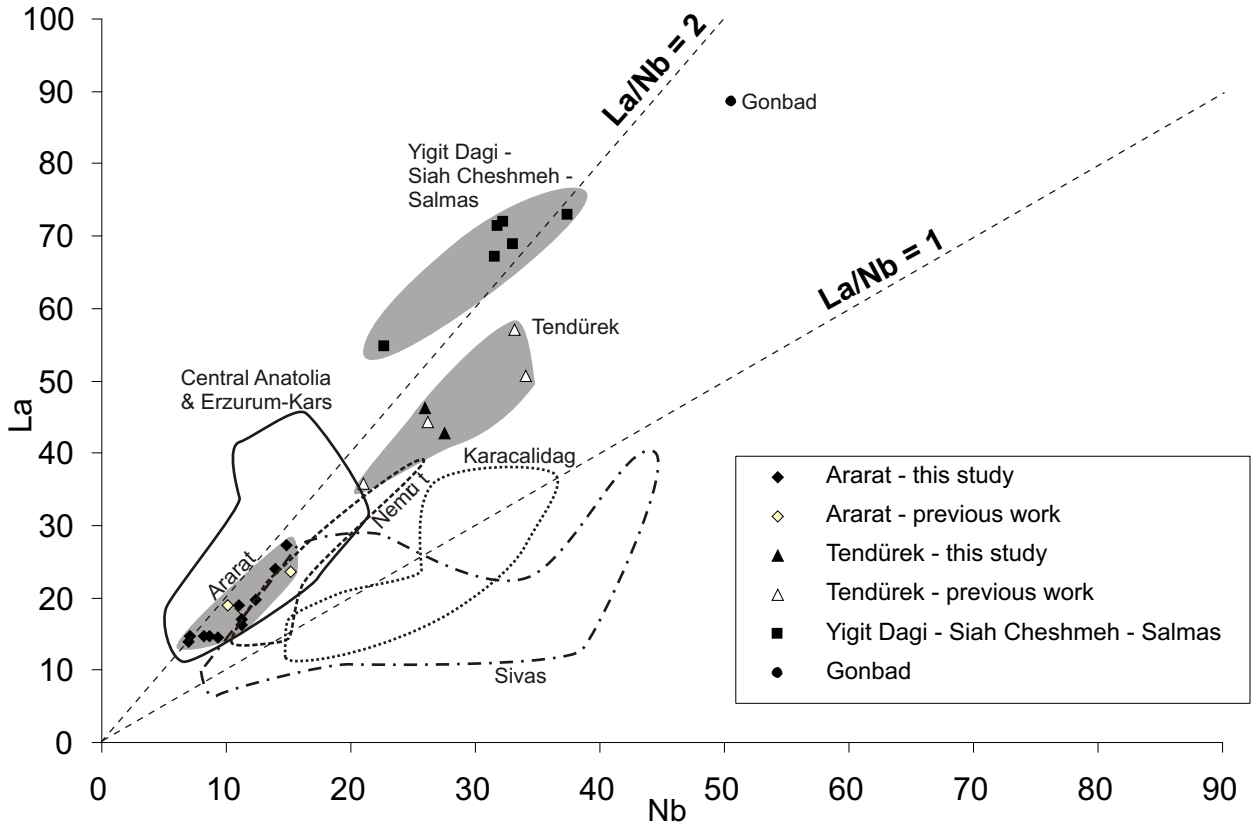
La
Nb
La/Nb = 2
La/Nb = 1
Gonbad
Yigit Dagi -
Siah Cheshmeh -
Salmas
Tendürek
Central Anatolia
& Erzurum-Kars
Karacalidag
Nemrut
Ararat
Sivas
Ararat - this study
Ararat - previous work
Tendürek - this study
Tendürek - previous work
Yigit Dagi - Siah Cheshmeh - Salmas
Gonbad

Fig. 5

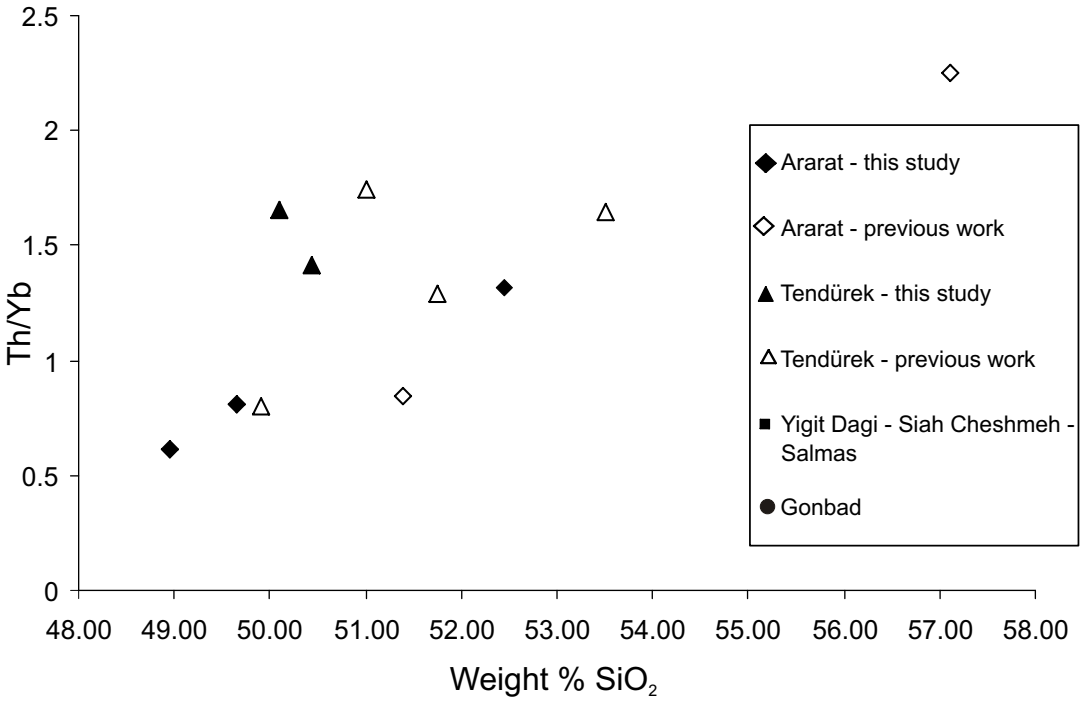
2.5
2
1.5
1
0.5
0
Th/Yb
48.00
49.00
50.00
51.00
52.00
53.00
54.00
55.00
56.00
57.00
58.00
Weight % SiO2
Ararat - this study
Ararat - previous work
Tendürek - this study
Tendürek - previous work
Yigit Dagi - Siah Cheshmeh - Salmas
Gonbad

Fig. 6

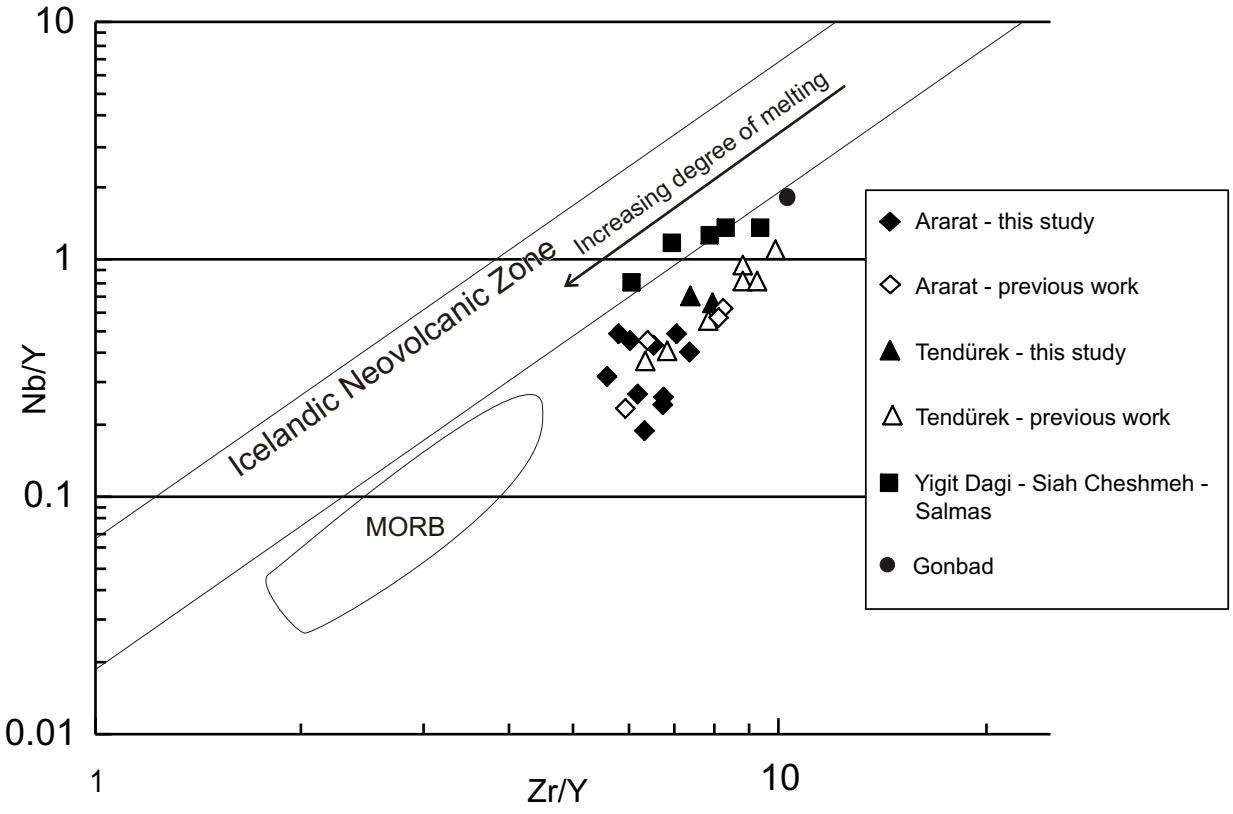
10
1
0.1
0.01
Nb/Y
1
Zr/Y
10
Icelandic Neovolcanic Zone
Increasing degree of melting
MORB
Ararat - this study
Ararat - previous work
Tendürek - this study
Tendürek - previous work
Yigit Dagi - Siah Cheshmeh - Salmas
Gonbad

Fig. 7

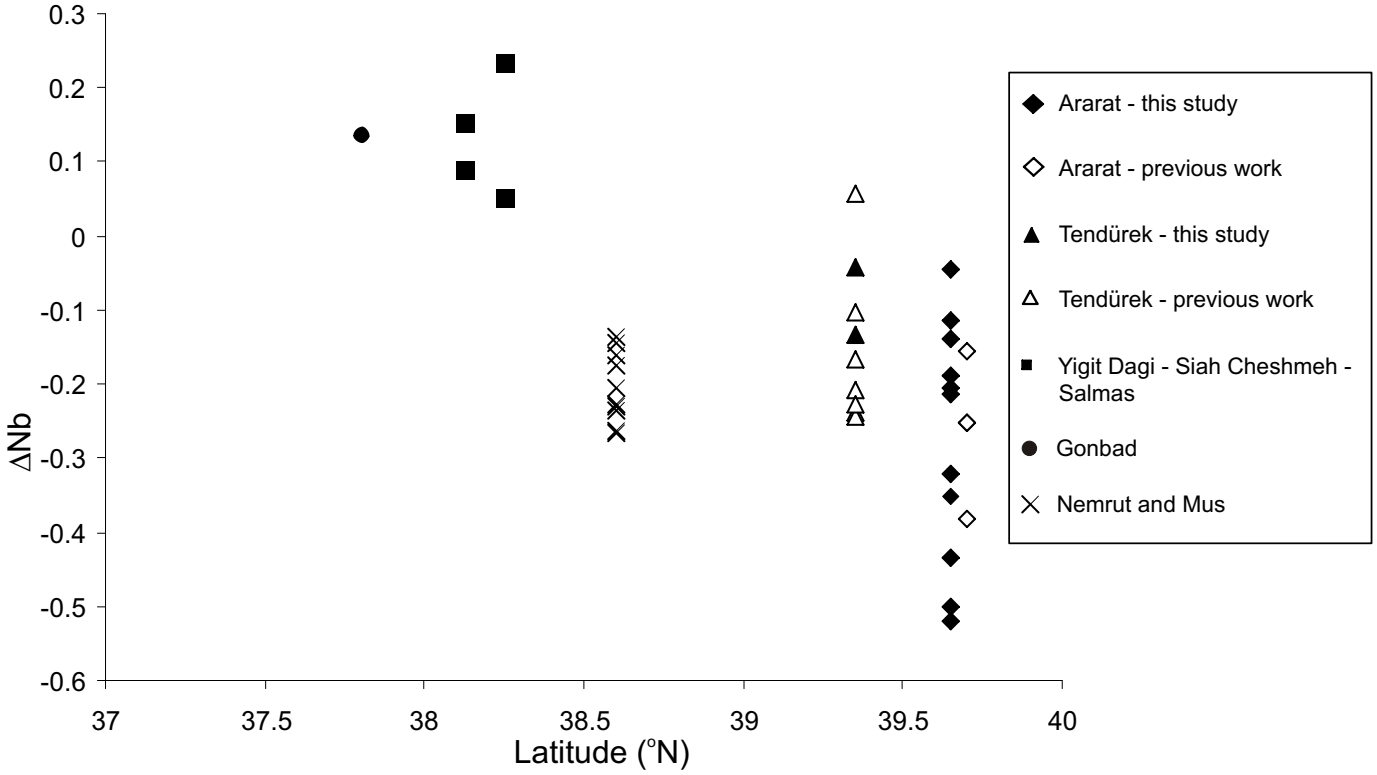
0.3
0.2
0.1
0
-0.1
-0.2
-0.3
-0.4
-0.5
-0.6
ΔNb
37
37.5
38
38.5
39
39.5
40
Latitude (°N)
Ararat - this study
Ararat - previous work
Tendürek - this study
Tendürek - previous work
Yigit Dagi - Siah Cheshmeh - Salmas
Gonbad
Nemrut and Mus

Fig. 8

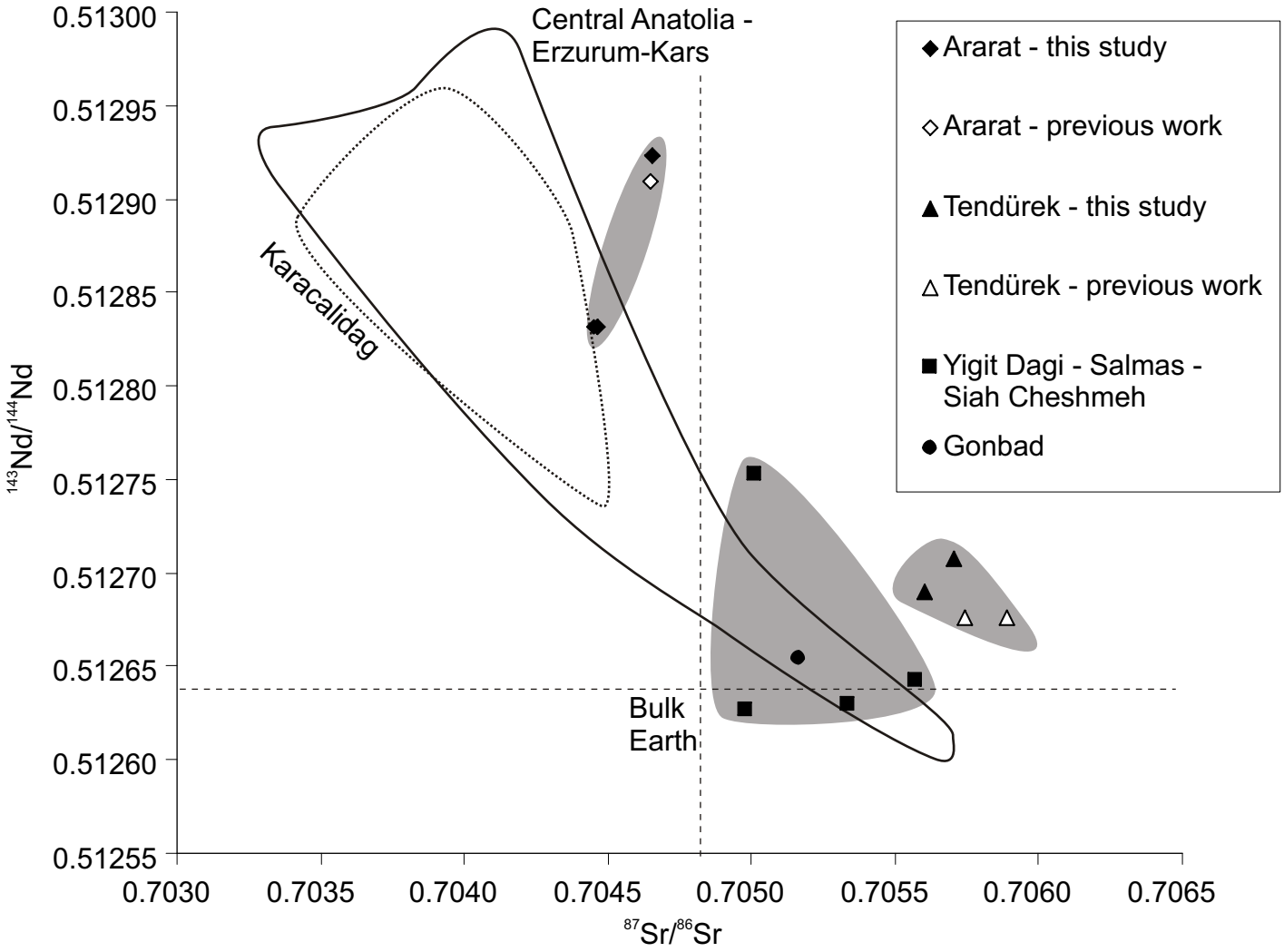
0.51300
0.51295
0.51290
0.51285
0.51280
0.51275
0.51270
0.51265
0.51260
0.51255
143Nd/144Nd
0.7030
0.7035
0.7040
0.7045
0.7050
0.7055
0.7060
0.7065
87Sr/86Sr
Central Anatolia -
Erzurum-Kars
Karacalidag
Bulk
Earth
Ararat - this study
Ararat - previous work
Tendürek - this study
Tendürek - previous work
Yigit Dagi - Salmas -
Siah Cheshmeh
Gonbad

Fig. 9

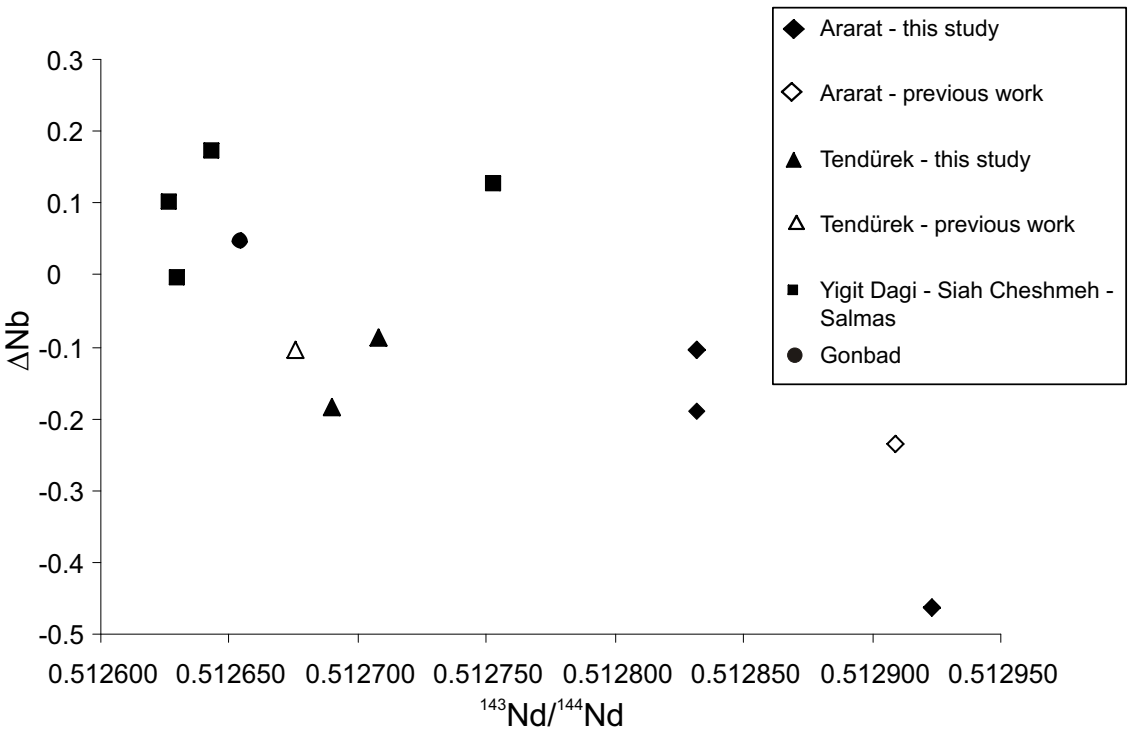
Ararat - this study
Ararat - previous work
Tendürek - this study
Tendürek - previous work
Yigit Dagi - Siah Cheshmeh - Salmas
Gonbad
ΔNb
0.3
0.2
0.1
0
-0.1
-0.2
-0.3
-0.4
-0.5
0.512600
0.512650
0.512700
0.512750
0.512800
0.512850
0.512900
0.512950
143Nd/144Nd

Fig. 10

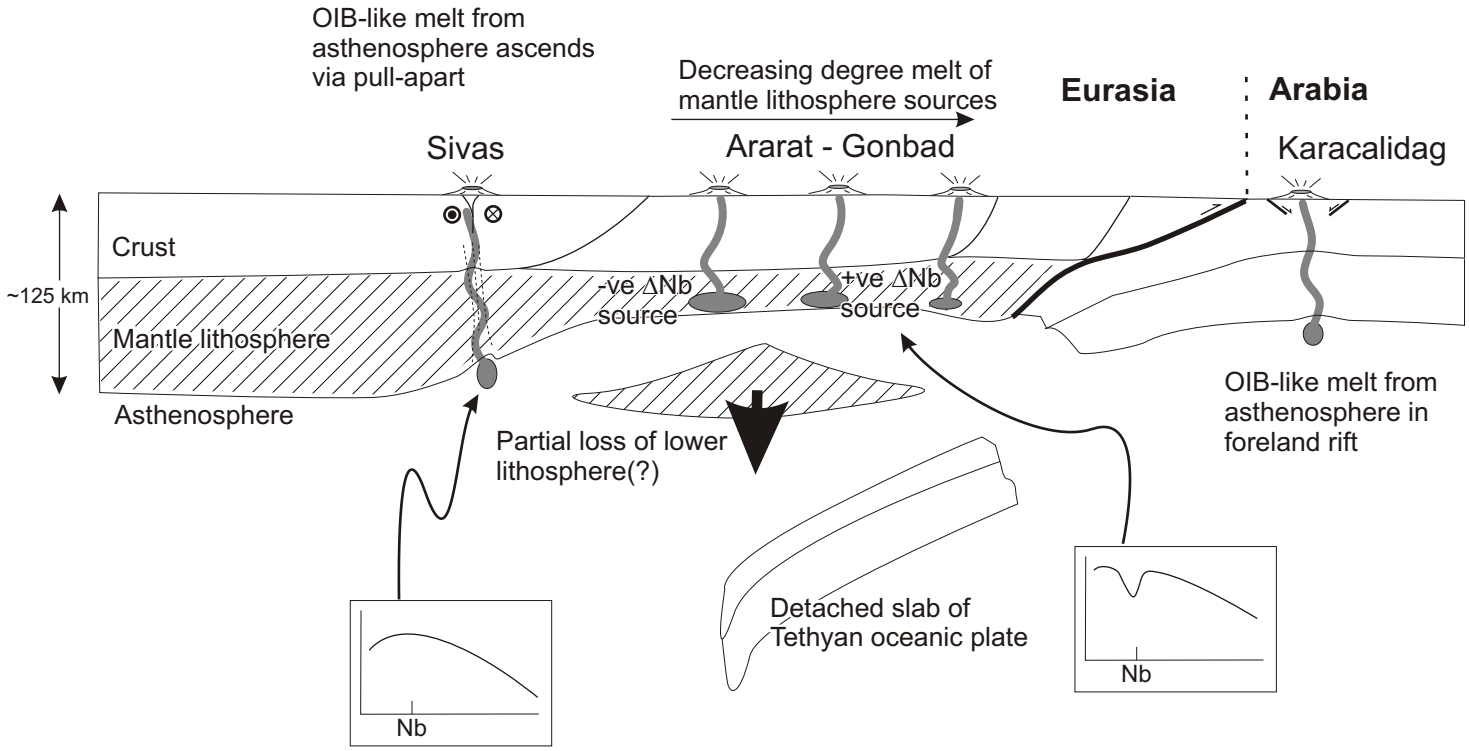
OIB-like melt from
asthenosphere ascends
via pull-apart
Decreasing degree melt of
mantle lithosphere sources
Eurasia
Arabia
Sivas
Ararat - Gonbad
Karacalidag
~125 km
Crust
Mantle lithosphere
Asthenosphere
-ve ΔNb
source
+ve ΔNb
source
OIB-like melt from
asthenosphere in
foreland rift
Partial loss of lower
lithosphere(?)
Detached slab of
Tethyan oceanic plate
Nb
Nb

Fig. 11

Table

Click here to download Table: Table 1.pdf

Sample No.	Mu 2.1	Mu 3.9	Mu 5.10	Mu 6.11	Mu 7.12	Mu 8.13	Mu 9.14	Mu 10.15	Mu 11.16	Mu 12.17	Mu 13.18	Mu 14.19	Mu 15.20	Mu 15.21	Mu 15.22	Mu 16.23	Mu 17.24	Mu 18.25	Mu 20.26	RK 4
Centre	Ararat	Ararat	Ararat	Ararat	Ararat	Ararat	Ararat	Ararat	Tendurek	Tendurek	Siah Cheshmeh	Yigit Dagi	Salmas	Salmas	Salmas	Yigit Dagi	Ararat	Ararat	Ararat	Gonbad
Rock type	basalt	basalt	basalt	andesite	trach-and	andesite	andesite	basalt	hawaiite	hawaiite	basalt	hawaiite	basalt	basalt	trach-and	hawaiite	hawaiite	basalt	basalt	mugearite
Major elements (wt. %)																				
SiO_2	50.38	50.19	49.81	52.45	54.95	55.43	53.67	50.35	50.43	50.10	49.03	52.21	48.11	48.71	59.17	46.00	51.40	48.95	49.64	48.23
TiO_2	1.76	1.90	1.77	1.27	1.26	1.14	1.30	1.54	2.21	2.05	1.44	1.23	1.32	1.19	0.81	1.50	2.17	1.60	1.67	1.73
Al_2O_3	17.10	17.19	16.95	16.15	16.58	16.17	15.97	16.44	17.72	17.91	14.74	16.02	13.74	13.79	16.03	14.78	16.93	16.37	16.09	17.95
Fe_2O_3	9.56	10.18	9.63	9.03	8.21	7.80	8.42	9.89	11.52	11.47	8.65	7.48	8.99	8.26	4.71	9.47	10.41	8.86	9.84	9.20
MnO	0.15	0.16	0.15	0.14	0.13	0.13	0.14	0.16	0.17	0.18	0.12	0.13	0.14	0.14	0.09	0.16	0.16	0.14	0.16	0.15
MgO	6.01	5.30	6.10	6.68	5.64	5.93	6.05	7.57	3.85	4.21	6.16	6.58	11.46	9.92	2.23	8.47	5.31	5.16	6.93	4.67
CaO	8.65	8.42	9.10	8.10	7.65	7.56	8.03	8.70	7.06	7.37	12.31	8.67	9.64	9.96	5.59	11.43	8.11	10.61	9.14	8.23
Na_2O	4.83	4.92	4.65	4.16	4.45	4.27	4.14	4.50	5.61	5.39	3.54	4.24	3.40	3.75	4.78	3.94	5.02	4.49	4.51	5.13
K_2O	0.79	0.64	0.71	0.99	1.29	1.12	1.18	1.03	1.59	1.63	1.36	2.73	2.01	2.22	3.93	1.99	0.68	0.55	1.06	2.99
P_2O_5	0.38	0.28	0.35	0.26	0.28	0.30	0.32	0.44	0.76	0.75	0.80	0.57	0.76	0.73	0.59	0.81	0.31	0.26	0.42	1.33
SO_3	0.40	0.03	0.04	0.02	0.02	0.01	0.27	0.03	0.02	0.04	0.02	0.03	0.02	0.06	0.06	0.03	0.05	0.27	0.08	0.05
L.O.I.	0.45	0.29	0.89	-0.04	0.06	0.11	0.57	-0.03	-0.48	-0.38	1.27	0.31	0.40	1.45	1.95	1.21	0.10	3.14	0.45	0.84
Total	100.46	99.50	100.14	99.23	100.50	99.97	100.07	100.64	100.47	100.71	99.44	100.18	100.00	100.18	99.94	99.79	100.67	100.41	99.98	100.50
Trace elements (ppm)																				
Sc	21	26	25	22	21	25	24	22	14	12	18	16	21	23	8	24	32	20	23	10
V	159	146	153	165	149	138	144	178	188	169	139	147	160	144	74	198	181	155	184	168
Cr	107	36	116	223	111	176	132	211	7	2	255	190	518	436	14	295	41	43	197	6
Co				37.1					29.1	32.3	28.2	29.9	48.0			40.6		33.4	39.2	26.3
Ni	62	39	66	148	69	79	79	97	21	23	170	110	354	243	8	167	39	59	156	11
Cu				47.0					25.6	23.4	70.8	33.7	52.1			49.6		36.0	46.0	16.5
Zn				74.9					131.3	130.5	73.8	71.7	78.2			82.8		73.7	85.8	90.4
Ga				16.8					20.7	20.5	16.5	17.0	15.5			16.3		17.1	16.7	18.2
Rb	11	9	11	19	31	28	29	16	20	25	9	65	47	58	128	44	10	7	15	50
Cs				0.6					0.1	0.5	2.1	3.7	1.6			3.8		0.2	0.3	1.1
Ba	271	171	175	288	379	366	348	323	435	567	761	722	799	810	940	851	229	213	309	924
Sr	564	492	519	364	387	376	376	658	581	652	1724	839	1113	1125	916	1066	460	523	571	1983
Y	32	31	27	25	29	23	26	31	38	38	27	24	24	24	20	28	37	27	29	28
Zr	197	211	204	149	187	163	174	179	268	300	171	211	191	203	252	184	234	172	172	253
Hf				3.33					5.79	5.91	3.59	4.50	4.09			3.90		3.64	3.71	5.06
Nb	9	8	11	10	12	11	11	15	27	27	23	32	33	32	37	33	7	5	12	47
Ta				0.58					1.27	1.29	1.12	1.75	1.80			1.69		0.33	0.66	2.41
La	15	15	16	16.08	20	17	19	27	37.07	39.86	54.83	61.94	66.11	72	73	61.25	15	11.05	20.79	82.02
Ce				31.85					73.50	78.47	108.17	111.26	125.94			113.70		26.05	43.98	155.12
Pr				4.11					9.41	9.90	13.51	12.55	14.81			13.39		3.74	5.81	18.32
Nd	20	23	22	17.52	20	18	19	26	38.45	39.85	52.45	44.92	54.33	53	47	49.49	26	17.33	24.34	67.09
Sm				3.98					7.49	7.72	8.50	7.06	8.18			7.92		4.19	5.19	9.91
Eu				1.29					2.18	2.24	2.30	1.81	2.12			2.15		1.46	1.66	2.60
Gd				4.45					7.14	7.14	6.39	5.19	5.68			6.19		4.84	5.47	6.71
Tb				0.72					1.10	1.10	0.87	0.77	0.80			0.89		0.78	0.85	0.94
Dy				4.20					6.36	6.41	4.71	4.27	4.34			4.97		4.57	4.94	5.04
Ho				0.86					1.28	1.29	0.89	0.82	0.81			0.94		0.93	1.00	0.95
Er				2.32					3.41	3.47	2.29	2.13	2.04			2.43		2.49	2.70	2.41
Tm				0.36					0.54	0.55	0.34	0.33	0.31			0.38		0.39	0.43	0.37
Yb				2.25					3.31	3.41	2.15	2.04	1.89			2.29		2.40	2.61	2.25
Lu				0.36					0.54	0.56	0.35	0.33	0.29			0.36		0.40	0.43	0.37
Pb	2	4	4	5.27	6	4	9	1	9.72	10.55	13.19	13.68	8.96	8	21	9.46	5	3.23	4.36	10.96
Th	7	7	6	2.97	6	9	9	7	4.67	5.65	6.72	17.30	11.26	15	32	11.30	3	1.48	2.10	10.87
U				1.07					0.62	1.41	1.79	3.06	2.25			2.34		0.81	0.62	2.34
$^{87}Sr/^{86}Sr$				0.704452					0.705705	0.705600	0.705008	0.705338	0.704979			0.705570		0.704657	0.704461	0.705163
2SE				0.000010					0.000010	0.000010	0.000008	0.000009	0.000009			0.000008		0.000011	0.000010	0.000008
$^{143}Nd/^{144}Nd$				0.512832					0.512708	0.512690	0.512753	0.512630	0.512627			0.512643		0.512923	0.512832	0.512654
2SE				0.000009					0.000006	0.000006	0.000006	0.000009	0.000008			0.000008		0.000014	0.000008	0.000007

Table 1. Major, trace element and isotopic data for volcanic samples from NW Iran. Centres are shown in Fig. 1.